Article:
Sharpe, G.J. and Maflahi, N. (2006) Homogeneous explosion and shock initiation for a three-step chain-branching reaction model. Journal of Fluid Mechanics, 566. pp. 163-194. ISSN 0022-1120

https://doi.org/10.1017/S0022112006001844

J. Fluid Mech. (2006), *vol.* 566, *pp.* 163–194.
doi:10.1017/S0022112006001844 Printed in the United Kingdom

Homogeneous explosion and shock initiation for a three-step chain-branching reaction model

By GARY J. SHARPE[1] AND NABEIL MAFLAHI[2]

[1]School of Mechanical Engineering, University of Leeds, Leeds, LS2 9JT, UK

[2]School of Computing and Information Technology, University of Wolverhampton, Wolverhampton, WV1 1SB, UK

(Received 30 August 2005 and in revised form 3 April 2006)

The role of chain-branching cross-over temperatures in shock-induced ignition of reactive materials is studied by numerical simulation, using a three-step chain-branching reaction model. In order to provide insight into shock initiation, the simpler problem of a spatially homogeneous explosion is first considered. It is shown that for ratios of the cross-over temperature to the initial temperature, T_B, sufficiently less than unity, the homogeneous explosion can be quantitatively described by a widely used two-step model, while for T_B sufficiently above unity the homogeneous explosion can be effectively described by the standard one-step model. From the matchings between these homogeneous-explosion solutions, the parameters of the reduced models are identified in terms of those of the three-step model. When T_B is close to unity, all the reactions of the three-step model have a leading role, and hence in this case the model cannot be reduced further. In the case of shock initiation, for T_B (which is now the ratio of the cross-over temperature to the initial shock temperature) sufficiently below unity, the three-step solutions are qualitatively described by those of the matched two-step model, but there are quantitative differences due to the assumption in the reduced model that a purely chain-branching explosion occurs instantaneously. For T_B sufficiently above unity, the matched one-step model is found to effectively describe the way in which the heat release and fluid dynamics couple. For T_B close to unity, the competition between chain branching and chain termination is important from the outset. In these cases the speed at which the forward moving explosion wave that emerges from the piston is sensitive to T_B, and changes from supersonic to subsonic for a value of T_B just below unity.

1. Introduction

An important issue from the perspective of safety (storage and handling) of fuels and explosives is how they respond to shock waves, e.g. how a shock may transition into a detonation wave. In gases, the initiating shock may be produced by driving a piston into the fuel or equivalently by the reflection of a weak shock from a confining wall (Meyer & Oppenheim 1971). In shock initiation experiments on liquid and solid explosives, the shock is produced by a flier plate which is fired at high velocity into the explosive from a gas gun (e.g. Gustavsen *et al.* 2002; Sheffield, Engelke & Alcon 1989).

The majority of work on the theory of shock initiation has employed a standard one-step Arrhenius reaction model (Sharpe & Short 2004; Short & Dold 2002; Nikiforakis & Clarke 1996; Singh & Clarke 1992; Blythe & Crighton 1989; Kapila & Dold

1989; Jackson & Kapila 1985). For this model, the shock-to-detonation transition mechanisms are well understood from these analytical and numerical studies. The evolution begins with an induction stage, during which the shocked material remains close to the initial state but evolves due to a small amount of heat release. This induction stage is then followed by a thermal runaway event at the piston, which signals that the material there subsequently burns rapidly to complete reaction. This thermal runaway event is just the first in a sequence of local explosions, since the induction stage evolution sets up a gradient in induction times due to the passage of the shock. The point of thermal runaway hence moves away from the piston face as each particle explodes in turn. A thin explosion zone thus subsequently propagates away from the piston. This reaction wave consists of part of a quasi-steady weak detonation (a shockless wave which is supersonic throughout in its own rest frame), possibly followed by an unsteady region and a quasi-steady subsonic fast flame. As the activation energy increases, the weak detonation part of the reaction wave grows, and in the high-activation-energy asymptotic limit, it consists entirely of the weak detonation. The wave has an initially infinite speed but decelerates very rapidly. Once it reaches the Chapman–Jouguet (CJ) speed, a sonic point appears at the rear of the weak detonation. This results in a secondary shock forming, which subsequently accelerates and propagates rapidly through the remaining part of the weak detonation ahead, transforming it into a strong detonation. As the activation energy is increased, the point where secondary shock and subsequent strong detonation appear rapidly moves closer to the piston. In the high-activation-energy limit they appear extremely close to the piston.

Although the one-step model shock-initiation picture is complete, such a model cannot properly describe how the heat is released in many real explosives, in which the chemistry is governed by chain-branching reactions. The chemistry in these fuels typically gives reaction histories consisting of a definite induction stage followed by a main reaction stage in which the majority of heat is released. The ratio of the time or length scales of these two stages depends both on the fuel and on the initial conditions. The one-step model cannot reproduce such reaction structures, except when the main reaction zone is exponentially short in comparison to the induction stage. Importantly, it has been shown that the evolution process can depend qualitatively on the reaction zone structure and hence the choice of reaction model (Sharpe 2002).

For simple chain-branching models, early time analyses (Sharpe 2002; Dold & Kapila 1991) show that, after an induction time, a chain-branched runaway occurs at the piston. The thin chain-branching explosion region subsequently propagates away from the piston at subsonic speeds, compared to the supersonic thermal runaway wave in the one-step model. The result is that, when chain-branching dominates in the explosion region, the shock initiation evolution never involves supersonic weak detonations which are the main feature in the one-step case. Sharpe (2002) then investigated the complete evolution using a very simple two-step chain-branching chemistry model, which consists of a thermally neutral induction time step followed by a state-insensitive exothermic main heat release stage. Sharpe (2002) found that, subsequent to the chain-branching explosion at the piston, the solution consists of three regions, which are, as one moves back from the shock to the piston: (i) an undisturbed induction region, (ii) an unsteady, disturbed induction region, which terminates with the instantaneous chain-branching explosion, and (iii) a subsonic fast-flame main reaction wave.

The subsequent evolution of this three-stage structure depends sensitively on the ratio of the main reaction time to the initial induction time (Sharpe 2002). For rapid

main reaction stage times, a secondary shock forms at the head of the disturbed induction zone region, very quickly and near the piston. This shock then rapidly amplifies, coupling with the fast-flame reaction zone behind it, to form a strong detonation. For more moderate main reaction times (comparable with the initial induction time), a secondary shock forms later and further from the piston. While this secondary shock is still amplified by the following exothermic reactions, it may not have time to reach a fully developed detonation before the secondary shock collides with the leading shock. For long main reaction times, no secondary shock forms and instead the reaction zone couples directly with the leading shock, so that the growth occurs smoothly and principally at or just behind the shock.

In this paper, shock initiation is investigated using a more realistic three-step chain-branching chemistry model. This is the simplest model that contains all the main features of chain-branching chemistry, including the concept of cross-over temperatures (which the two-step model lacks). The three-step model has been used in several studies of ignition and detonation problems (Blythe, Kapila & Short 2005; Maflahi 2004, 2005; Short & Sharpe 2005; Ng & Lee 2003; Short, Kapila & Quirk 1999; Short & Quirk 1997; Dold & Kapila 1991). The main purpose of this paper is to determine if and how the solutions obtained using the three-step model differ from those using the simpler one-step and two-step models, and to examine the role of the chain-branching cross-over temperature in shock-induced ignition.

Previous studies have also shown that, for a given chemistry model, the solutions of the simpler homogeneous (constant-volume) explosion problem provide a number of predictions and fundamental insights into the shock initiation problem. Hence we also consider the homogeneous explosion for the three-step model in order to provide understanding of the dependence of shock initiation on the chain-branching crossover temperature. Furthermore, our homogeneous explosion study also shows how the asymptotic results given in Blythe *et al.* (2005) and Maflahi (2004, 2005) for the three-step model can be used to directly relate the model parameters to those of one- or two-step models, at least within particular regimes of the value of the chain-branching cross-over temperature.

The plan of the paper is as follows: the three-step model is summarized in § 2; homogeneous explosions are considered in § 3; shock-initiation results are given in § 4; § 5 contains the conclusions.

2. The three-step reaction model

Here we briefly summarize the three-step kinetics model which is described in detail in Short & Quirk (1997). The three reaction stages are as follows: (i) a chain-initiation step, in which fuel, F, is converted slowly into free radicals, Y, at a rate of reaction R_I; (ii) a chain-branching step in which the radicals combine with fuel to produce more radicals, F+Y→2Y, at a rate R_B; (iii) a chain-termination or recombination step in which the radicals are converted into reaction products, P, at rate R_C. The reaction rates are assumed to be of Arrhenius form,

$$R_I = k_I f \exp\left(-\frac{\theta_I}{T}\right), \quad R_B = k_B f y \rho \exp\left(-\frac{\theta_B}{T}\right), \quad R_C = k_C y \exp\left(-\frac{\theta_C}{T}\right), \quad (2.1)$$

where k_I, k_B and k_C are the chain-initiation, -branching and -termination rate constants, respectively, θ_I, θ_B and θ_C are the activation energies, T is the temperature, ρ the density and f and y the fuel and radical mass fractions respectively (the mass fraction of products, z, is then given by conservation of mass as $z = 1 - f - y$).

In any real chemical reaction, there will be multiple individual initiation, branching and re-combination reactions occurring. It is important to note that in the simplified three-step model, it is assumed that all the chain-initiation reactions can effectively be described by (or combined into) a single global initiation step, and similarly for the branching and termination reactions (Blythe *et al.* 2005). The important point for high-speed reactive flow problems is to correctly capture how the heat is released and couples to the flow, rather than how any individual reaction proceeds.

We make the standard further simplifying assumptions (Blythe *et al.* 2005; Maflahi 2005; Short & Sharpe 2005; Ng & Lee 2003; Short *et al.* 1999; Short & Quirk 1997) that the termination step is rate independent, $\theta_C = 0$, since typically chain termination is only weakly temperature dependent (Short & Quirk 1997), and that the initiation and branching steps are thermally neutral (in reality the initiation steps tend to be only weakly endothermic (Short & Quirk 1997)). Note that this second assumption is a good approximation for hydrogen mixtures, whereas in hydrocarbons such as acetylene, the branching steps may also release significant heat (Varatharajan & Williams 2001). We intend to investigate how exothermic branching affects the solutions as an extension in the future, but here we consider only the basic three-step model properties. Hence all of the chemical heat, Q, is released in the termination step.

The rate constants, k_I and k_B, are then re-defined in terms of *cross-over temperatures*, T_I and T_B, by

$$k_I = k_C \exp\left(\frac{\theta_I}{T_I}\right), \quad k_B = k_C \exp\left(\frac{\theta_B}{T_B}\right), \tag{2.2}$$

so that the reaction rates can be rewritten as

$$R_I = k_C f \exp\left[\frac{1}{\epsilon_I}\left(\frac{1}{T_I} - \frac{1}{T}\right)\right], \quad R_B = k_C f y \rho \exp\left[\frac{1}{\epsilon_B}\left(\frac{1}{T_B} - \frac{1}{T}\right)\right], \quad R_C = k_C y, \tag{2.3}$$

where here we have also defined the standard inverse activation energies, $\epsilon_I = \theta_I^{-1}$, $\epsilon_B = \theta_B^{-1}$. It is now clear that the chain-branching cross-over temperature, T_B, is the temperature at which the branching rate multiplier becomes equal to that of the termination rate. Similarly T_I is the temperature at which the initiation rate multiplier is equal to that of the termination step. Finally, we make the standard realistic assumptions (Short & Quirk 1997) that $T_B < T_{\mathrm{ad}} < T_I$ (where T_{ad} is the adiabatic explosion temperature) and $\epsilon_I \ll \epsilon_B$ (the activation energy of the initiation step is typically much larger than that of the branching step).

3. Homogeneous explosion

Here we briefly examine and review the homogeneous (spatially uniform) constant-volume explosion solutions of the three-step model, especially the dependence on T_B. Homogeneous explosion solutions can provide useful *a priori* insights into the parametric dependences of the shock initiation solutions (Short & Sharpe 2004). We then show that the homogeneous-explosion solutions allow the three-step model to be directly identified with the simpler (reduced) one-step or two-step models in certain parameter regimes. Given these matchings between models, a number of further predictions of the shock initiation solutions can then be obtained from the previous one-step and two-step model studies of Sharpe & Short (2004) and Sharpe (2002) (see § 4.1).

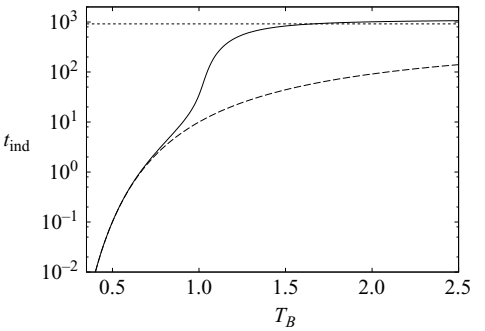

FIGURE 1. Induction time (time to $f = 0.5$) of the homogeneous explosion (logarithmic scale) against T_B. Also shown is the leading-order high-activation-energy asymptotic induction times for $T_B - 1 = O(1) < 0$ (dashed line) and $T_B - 1 = O(1) > 0$ (dotted line).

For the spatially uniform, constant-volume scenario, the (dimensionless) governing equations are simply

$$\frac{\mathrm{d}f}{\mathrm{d}t} = -R_I - R_B = -f \exp\left[\frac{1}{\epsilon_I}\left(\frac{1}{T_I} - \frac{1}{T}\right)\right] - fy \exp\left[\frac{1}{\epsilon_B}\left(\frac{1}{T_B} - \frac{1}{T}\right)\right], \tag{3.1a}$$

$$\frac{\mathrm{d}y}{\mathrm{d}t} = R_I + R_B - R_C = f \exp\left[\frac{1}{\epsilon_I}\left(\frac{1}{T_I} - \frac{1}{T}\right)\right] + fy \exp\left[\frac{1}{\epsilon_B}\left(\frac{1}{T_B} - \frac{1}{T}\right)\right] - y, \tag{3.1b}$$

$$\frac{\mathrm{d}T}{\mathrm{d}t} = \beta y. \tag{3.1c}$$

Here t is a dimensionless time based on the termination-rate time scale, defined by $t = \tilde{k}_C \tilde{t}$ (where a tilde denotes a dimensional quantity). The temperature and the (constant) density have been scaled with their values in the initial state, i.e. $T = \tilde{T}/\tilde{T}_0$, where the zero subscript denotes initial values. Since only the termination step releases heat in the basic three-step model, the temperature is governed simply by (3.1c), where $\beta = (\gamma - 1)Q$, γ is the ratio of specific heats and Q is the dimensionless heat of reaction. Adding equations (3.1a)–(3.1c) and integrating gives

$$T = 1 + \beta(1 - f - y) = 1 + \beta z. \tag{3.2}$$

Thus the adiabatic (final, all products) temperature is $T_{\mathrm{ad}} = 1 + \beta$.

The initial conditions are $f(0) = 1$, $y(0) = 0$ and $T(0) = 1$. We define

$$e_B = \exp\left[\frac{1}{\epsilon_B}\left(\frac{1}{T_B} - 1\right)\right], \quad e_I = \exp\left[\frac{1}{\epsilon_I}\left(\frac{1}{T_I} - 1\right)\right], \tag{3.3}$$

which are the initial values of the branching and initiation rate multipliers, respectively. Throughout this paper, the following parameter set has been used:

$$\epsilon_I = 1/15, \quad \epsilon_B = 1/5, \quad T_I = 3, \quad Q = 4, \quad \gamma = 1.4, \tag{3.4}$$

and only the main parameter, T_B, varied.

Figure 1 shows the time at which the fuel fraction reaches a half (which we use here as a measure of the induction time, denoted by t_{ind}) as a function of T_B. From figure 1 it can be seen that there are three different T_B regimes of the induction time, and that the induction time varies most rapidly for initial temperature close to T_B.

Figure 2 shows the complete numerical solutions of the homogeneous-explosion problem for various T_B. Figure 2(a) shows that for $T_B = 0.6$, the overall reaction

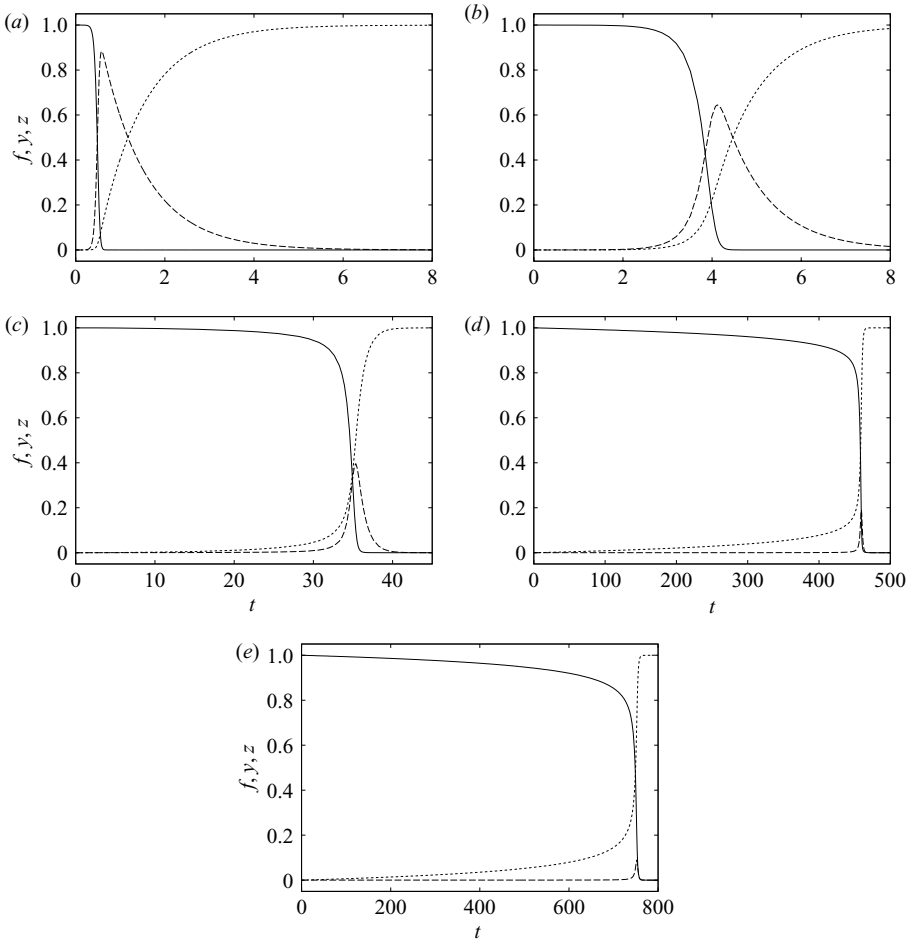

FIGURE 2. Fuel, f (solid lines), radical, y (dashed lines) and product, $z=(T-1)/\beta$ (dotted lines) mass fraction histories for the homogeneous explosions with (*a*) $T_B=0.6$, (*b*) $T_B=0.8$, (*c*) $T_B=1.0$, (*d*) $T_B=1.2$ and (*e*) $T_B=1.4$.

structure has three distinct stages. The first stage consists of an induction zone, and is followed by a chain-branching explosion zone in which the fuel is completely depleted and converted rapidly into radicals. Only a very small amount of products (and hence heat) is generated within this explosion region. Note that, in this paper, by 'explosion region', we are referring to the thin region where the fuel is consumed in a self-accelerating manner. Finally there is a chain termination stage where the radicals are converted into products and where the heat is released. The induction zone time is short compared to that of the termination stage. As T_B is decreased below 0.6, the induction stage becomes exponentially shorter, as can be seen in figure 1, while the mass fraction of radicals at the peak value rapidly approaches unity (Maflahi 2004).

As T_B begins to approaches unity from below, however, the distinct three-stage structure seen for lower values begins to break down. For example, figure 2(*b*) shows the structure for $T_B=0.8$. In this case, while the induction zone is still virtually thermally neutral, there is a noticeable buildup of products within the explosion region. Hence there is now a distinct overlap of the branching and termination

zones. The radical mass fraction peaks at $y = 0.644$ at which point $z = 0.294$. Thus the explosion region is no longer mainly chain branching in character, but is also partially thermal. For $T_B = 0.8$, the induction time and the termination-zone time scale are now comparable.

As T_B is further increased towards unity from below, the branching and termination regions overlap more and the radical peak decreases, while the induction zone rapidly becomes long on the termination time scales. Figure 2(*c*) shows the reaction structure when $T_B = 1$. In this case it can be seen that the induction zone is no longer thermally neutral, since a small decrease in the fuel fraction occurs before the explosion region, with a concomitant increase in products (and hence temperature), because now the termination reaction consumes radicals as they are produced by the initiation step. In the explosion region itself, there is a clear competition between branching and termination, with significant amounts of both radicals and products being produced. The radical and product fractions are comparable when the radicals peak. By the time all the fuel is consumed in the explosion region, about 80% of the mass is products. Hence now the explosion region has a very definite mixed chain-branching/thermal nature. In this case the induction zone is long compared to the overall termination length scale.

Figures 2(*d*) and 2(*e*) show the solutions for cases where T_B is larger than unity ($T_B = 1.2$ and 1.4, respectively). The induction zone is now very long compared to the termination zone. Indeed, note from figure 1 that the induction time initially increases exponentially rapidly as T_B is increased above unity. In these cases the structure consists of a thermally evolving induction stage, in which there is a more significant buildup of products (and heat) and depletion of fuel than for $T_B = 1.0$. The explosion region is now almost purely thermal in nature, with only a very small amount of radicals being produced. The radical production occurs near the end of the explosion, only once the local temperature reaches and then exceeds T_B. Thus the solution now resembles more a two-stage structure, consisting of a weakly evolving induction stage followed by a thermal explosion in which fuel is converted mainly into products. As T_B increases, the peak radical fraction reduces further. The induction time continues to increase with T_B initially, but then becomes independent of T_B for large enough values (figure 1). This is because, for sufficiently large T_B, the branching rate is exponentially small compared to the termination rate at all times, and hence the branching rate parameters have virtually no role in the evolution.

3.1. $T_B < 1$: *matching to the two-step model*

The three-stage structure and its T_B dependence, when T_B is sufficiently below unity, is confirmed by a high-activation-energy asymptotic analysis for the case when $T_B - 1 = O(1) < 0$ as $\epsilon_B \to 0$ (Blythe *et al.* 2005; Maflahi 2004). The leading-order asymptotic structure in this case can be summarized as follows. The first asymptotic region is an induction stage (Region I), in which

$$\left.\begin{aligned} f &= 1 + \frac{e_I}{e_B}(1 - \exp(\tau)), \quad y = \frac{e_I}{e_B}(\exp(\tau) - 1), \\ T &= 1 + \beta\frac{e_I}{e_B^2}(\exp(\tau) - \tau - 1), \quad \tau = e_B t, \end{aligned}\right\} \tag{3.5}$$

and thus in which f, y and T remain exponentially close to their initial values (but with the T perturbation being of smaller order than the mass fractions). The second asymptotic region (Region II) is the chain-branching explosion stage where fuel is

converted rapidly into radicals, and in which

$$f = \frac{1}{1+\exp(\hat{\tau})}, \quad y = \frac{\exp(\hat{\tau})}{1+\exp(\hat{\tau})}, \quad T = 1 + \frac{\beta}{e_B}\ln(1+\exp(\hat{\tau})), \quad \hat{\tau} = e_B t - \ln\left(\frac{e_B}{e_I}\right). \tag{3.6}$$

Note the temperature perturbation still remains exponentially small in this region, while the mass fraction perturbations are $O(1)$. The third and final asymptotic region (Region III) is the chain-termination stage where the radicals are converted to products and heat. In this region f is exponentially small, and

$$y = \left(\frac{e_B}{e_I}\right)^{1/e_B}\exp(-t), \quad T = 1 + \beta\left(1 - \left(\frac{e_B}{e_I}\right)^{1/e_B}\exp(-t)\right). \tag{3.7}$$

The asymptotic theory predicts a leading-order induction time (time to the chain-branching explosion) as

$$t_{\mathrm{ind}} = \frac{1}{e_B}\ln\left(\frac{e_B}{e_I}\right) = \exp\left[\frac{1}{\epsilon_B}\left(1-\frac{1}{T_B}\right)\right]\left\{\frac{1}{\epsilon_B}\left(\frac{1}{T_B}-1\right) - \frac{1}{\epsilon_I}\left(\frac{1}{T_I}-1\right)\right\}. \tag{3.8}$$

The leading-order asymptotic solution gives excellent quantitative agreement with the full numerical results for finite activation energies, including the induction time, even for moderate values of the branching activation energy, such as the value of $\epsilon_B = 1/5$ used here (Blythe *et al.* 2005; Maflahi 2004). This is shown to be the case in figure 1, where the asymptotic induction times agree quantitatively with the numerical values provided T_B is in the relevant regime (sufficiently below unity). The leading-order asymptotics are quantitatively accurate because the correction term at the next order is exponentially small and thus numerically negligible (Blythe *et al.* 2005).

This analytical structure confirms that the explosion region is mainly chain branching in character, while the temperature has a two-stage structure. This indicates that a reduced two-step model should be able to describe well the way in which the heat is released in the three-step model. Indeed, such two-step models were developed precisely to mimic the main features of this class of reaction structure (e.g. Short 2001). Here we examine how the parameters of the two-step model used in Sharpe & Short (2002), Sharpe (2002), Short & Sharpe (2002), Short (2001) and Short & Bdzil (2003) can be set so that the way in which the heat is released precisely matches that of three-step model in the $T_B - 1 = O(1) < 0$ regime. This two-step model begins with a thermally neutral induction stage,

$$\frac{\mathrm{d}\xi}{\mathrm{d}t} = k_1^* \exp\left(-\frac{1}{\epsilon_2 T}\right) = k_1 \exp\left[\frac{1}{\epsilon_2}\left(1-\frac{1}{T}\right)\right], \tag{3.9}$$

where ξ is an induction time parameter, such that the end of the induction time for a particle occurs when $\xi = 1$ (with $\xi = 0$ in the completely unburnt state), k_1^* is a rate constant and ϵ_2 is an inverse activation energy. Here we have also defined a rescaled rate constant, k_1, by $k_1 = k_1^* \exp(-1/\epsilon_2)$ in order to give a form of the rate consistent with Sharpe & Short (2002) and Sharpe (2002).

When the induction time $\xi = 1$ is reached a purely chain-branching explosion is assumed to occur, where the fuel is *instantaneously* converted into radicals, i.e. the chain-branching explosion region is assumed to be infinitely thin in the two-step model. Hence once the induction time is over a main reaction (termination) stage

begins. This stage is governed by

$$\frac{\mathrm{d}\lambda}{\mathrm{d}t} = k_2(1-\lambda)H(\xi), \tag{3.10}$$

where λ is a reaction progress variable (with $\lambda = 0$ at the start of the second step and unity in the completely burnt (all product) state), k_2 is the rate constant and H is the Heaviside function (so that the main reaction stage does not begin until the end of the induction stage). As in the three-step model, all the heat is released in the termination stage. The temperature is thus given by $T = 1 + \beta\lambda$. Note that equations (3.9) and (3.10) have been non-dimensionalized in the same way as the three-step model, hence $k_1 = \tilde{k}_1/\tilde{k}_C$, etc. The main parameter of the two-step model is $k = k_2/k_1$ (Sharpe & Short 2002; Sharpe 2002; Short & Sharpe 2002; Short 2001; Short & Bdzil 2003), which determines the ratio of the induction time to the main reaction time.

For the two-step model, the homogeneous explosion has an analytic solution:

$$\xi = k_1 t, \quad t_{\mathrm{ind}}^{\mathrm{2step}} = \frac{1}{k_1}, \quad \lambda = 1 - \exp(k - k_2 t). \tag{3.11}$$

The induction time, ξ, is a lumped variable and hence cannot be readily identified with f or y in the three-step model. However, matching the homogeneous induction time with that of the three-step model in equation (3.8) gives

$$k_1 = k_1^* \exp\left(-\frac{1}{\epsilon_2}\right) = \exp\left[\frac{1}{\epsilon_B}\left(\frac{1}{T_B} - 1\right)\right]\left\{\frac{1}{\epsilon_B}\left(\frac{1}{T_B} - 1\right) - \frac{1}{\epsilon_I}\left(\frac{1}{T_I} - 1\right)\right\}^{-1}. \tag{3.12}$$

The induction times between the two models can thus be matched by choosing

$$\epsilon_2 = \epsilon_B, \quad k_1^* = k_B\left\{\frac{1}{\epsilon_B}\left(\frac{1}{T_B} - 1\right) - \frac{1}{\epsilon_I}\left(\frac{1}{T_I} - 1\right)\right\}^{-1}. \tag{3.13}$$

The activation energy in the two-step model is thus identified to be precisely that of the chain-branching reaction step, while the two-step induction-stage rate constant is a combination of both initiation and branching effects, consistent with the fact that the two-step induction stage is assumed to represent a lumped combination of initiation and branching reactions (Short 2001).

The chain-branching explosion zone (Region II in the three-step structure) is replaced by an instantaneous change of fuel into radicals in the two-step model. In the termination region, given the matched values for ϵ_2 and k_1^* above, the temperatures in the main reaction stage of the two models can then be matched by choosing $k_2 = 1$, cf. equations (3.11) and (3.7). One then also notes that the reaction progress variable λ is simply the product mass fraction, z, of the three-step model. Importantly, given these parameter matches, the main parameter of the two-step model, k, is determined in terms of T_B by

$$k = \frac{1}{e_B}\ln\left(\frac{e_B}{e_I}\right). \tag{3.14}$$

Figure 3 shows comparisons between the temperature histories for the two-step and three-step models given the parameter matchings above, for the cases $T_B = 0.6$ and $T_B = 0.8$, for which $k = 0.476$ and 3.22, respectively. For $T_B = 0.6$ the agreement is quantitatively excellent. The only difference can be seen by close inspection near the chain-branching explosion region. For the two-step model, there is a discontinuity of

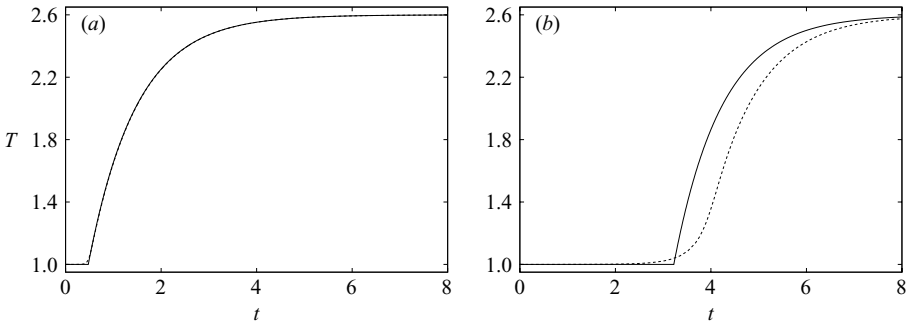

FIGURE 3. Temperature histories from the two-step (solid lines) and three-step (dotted lines) model homogeneous explosion solutions for (*a*) $T_B = 0.6$ ($k = 0.476$) and (*b*) $T_B = 0.8$ ($k = 3.22$).

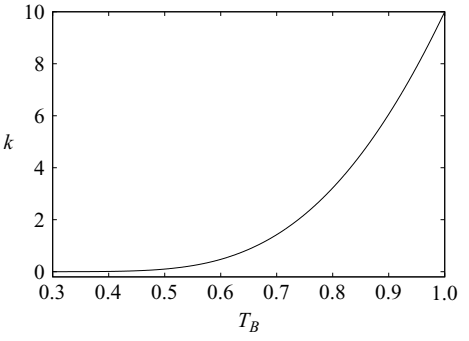

FIGURE 4. Two-step model parameter k as a function of T_B.

the temperature gradient at the induction time, due to the Heaviside switch in the heat release rate of equation (3.10). For the full three-step model, however, while the main chain-branching explosion region is thin, it is nevertheless temporally distributed, so that while there is a rapid change in the temperature gradients here, the temperature evolution is nevertheless smooth. For $T_B = 0.8$, the agreement between the two models is still qualitatively good, but the induction times no longer match. This is because for this value of T_B the explosion region in the three-step model is no longer mainly chain-branching in nature as assumed in the two-step model, but is also beginning to involve thermal effects. Hence one is moving outside the regime in which the assumptions and approximations inherent in the purely chain-branching two-step model are valid. In other words, reduction of the three-step model to the two-step model is only valid in the regime $T_B - 1 = O(1) < 0$.

However, the above matching between the two-step and three-step model also reveals a further important point. In studies using the two-step model, typically three regimes are considered (Sharpe & Short 2002; Sharpe 2002; Short 2001; Short & Bdzil 2003): $k \ll 1$, $k = O(1)$ and $k \gg 1$, corresponding to the main reaction (termination) time/length scale being long, comparable and short, respectively, on the induction time/length scale.

Figure 4 shows k as a function of T_B for the parameter set (3.4). As can be seen, although k can be made arbitrarily small by decreasing T_B, even when pushing the two-step matching well beyond its limit of applicability to $T_B = 1.0$, k remains less than 10. Hence the large-k limit, where the induction time is long, cannot be reached within the context of the three-step model. Even for general parameter values, equation (3.14)

shows that in the regime where the two-step model is applicable, $T_B - 1 = O(1) < 0$, k is always small since e_B is exponentially large. Even pushing T_B towards unity such that $e_B = O(1)$ and where the validity of the two-step model breaks down, equation (3.14) shows that then $k = O(1/\epsilon_I)$. Thus extremely large initiation activation energies (of the order of 100 to 1000) would be required to obtain values of k sufficiently large, e.g. the $k \gg 1$ values used in Sharpe (2002) and Sharpe & Short (2002), such that the termination stage is short compared to the induction stage. Thus the large-k regimes considered in Sharpe (2002), Short & Sharpe (2002), Short (2001) and Short & Bdzil (2003) are in fact not achievable within the context of the three-step model.

Indeed, figure 2 shows that in order to achieve induction zones which are long compared to the termination zone, T_B needs to be very close to or above unity. However, in these cases termination (and hence thermal) effects are important both within the induction stage and the explosion stage, and hence cannot be described by the purely chain-branching two-step model. These regimes are considered next.

However, this does not preclude the possibility of the large-k regime being achievable for chemistry models more complex than the three-step one. For example one could attempt to apply such a model to mixtures like methane which have very short main reaction stages. However, in such a case, a one-step model with sufficiently high activation energy could also reproduce the heat release structure. Given that the shock initiation dynamics of a two-step and one-step description are qualitatively different, care would have to be taken in deciding on the choice of model.

3.2. $T_B > 1$: *matching to the one-step model*

For T_B sufficiently above unity, we have seen that the explosion is mainly thermal in nature, with very little chain branching occurring. The relevant regime in the asymptotic analysis is $T_B - 1 = O(1) > 1$ as $\epsilon_I \to 0$. In this case the leading-order asymptotic induction time is (Blythe *et al.* 2005; Maflahi 2005)

$$t_{\mathrm{ind}} = \frac{\epsilon_I}{\beta e_I} = \frac{\epsilon_I}{\beta} \exp\left[\frac{1}{\epsilon_I}\left(1 - \frac{1}{T_I}\right)\right], \tag{3.15}$$

which now depends only on the chain-initiation rate parameters and is thus independent of those of the branching rate. This predicts an induction time which is now exponentially large compared to the termination stage time, since e_I remains exponentially small. Within this induction stage, the leading-order asymptotics predict that y is exponentially small, while the fuel mass fraction and temperature vary by an $O(\epsilon_I)$ amount: the leading-order solutions give

$$f = 1 + \frac{\epsilon_I}{\beta}\ln(1 - \beta\tau), \quad T = 1 - \epsilon_I \ln(1 - \beta\tau), \quad \tau = \frac{e_I}{\epsilon_I}t \tag{3.16}$$

(Blythe *et al.* 2005; Maflahi 2005).

The asymptotic induction time (3.15) is compared with the numerical finite-activation-energy values in figure 1. In agreement with the asymptotic predictions, the induction time does become independent of T_B for large enough values. However, the finite-activation-energy induction time for T_B sufficiently larger than unity is not in quantitative agreement with what the leading-order high-activation-energy asymptotics predict. This is because the higher-order correction is $O(\epsilon_I)$ (Blythe *et al.* 2005). Hence, unlike the $T_B - 1 = O(1) < 0$ case where the correction term is negligibly small, for $T_B - 1 = O(1) > 0$ the leading-order asymptotic solution is not quantitatively accurate for typical values used in finite-activation-energy calculations. For the one-step model, these differences between leading-order asymptotics and

finite-activation-energy solutions produce profound differences in the shock initiation scenario (Sharpe & Short 2004), and hence we expect the same to be true for the three-step model in this T_B regime.

However, the leading-order solution is still useful: note that the three-step induction-stage asymptotic solutions and induction time given in equations (3.15) and (3.16) are of precisely the same form as those of the high-activation-energy asymptotic solutions of the one-step model given in Kapila (1983). This suggests that, at least in the induction phase, the three-step model can be effectively described by the one-step model. Furthermore, the asymptotic analyses indicate how the parameters of the one-step model can be chosen so that the homogeneous-explosion structure matches that of the three-step model. The one-step model consists of a single reaction rate which converts fuel directly into products and releases the heat, given by

$$\frac{\mathrm{d}f}{\mathrm{d}t} = -k^* f \exp\left(-\frac{\epsilon}{T}\right), \tag{3.17}$$

where k^* is the rate constant, and ϵ the activation energy. For this model the leading-order induction time is (under the scalings used to non-dimensionalize the three-step model)

$$t_{\mathrm{ind}} = \frac{\epsilon}{\beta k^*} \exp\left(\frac{1}{\epsilon}\right). \tag{3.18}$$

(Kapila 1983). The one-step and three-step asymptotic induction times (3.15) and (3.18) can be matched if one makes the identifications

$$\epsilon = \epsilon_I, \quad \frac{1}{k^*} \exp\left(\frac{1}{\epsilon}\right) = \exp\left[\frac{1}{\epsilon_I}\left(1 - \frac{1}{T_I}\right)\right] \Rightarrow k^* = k_I. \tag{3.19}$$

Thus the leading-order induction solutions of the two models match if one identifies the rate constant and activation energy of the one-step model precisely as those of the chain-initiation step in the three-step model.

Given these parameter matches, the leading order asymptotic solutions of the one-step model in the induction stage also match those of the three-step model in equation (3.16) (Maflahi 2005). Furthermore, the next asymptotic region in both cases also match. This second region is a thermal explosion layer which occurs at $t = t_{\mathrm{ind}}$ (Blythe *et al.* 2005; Maflahi 2005; Kapila 1983). For example, in both models the thermal explosion region occurs on the time-scale $\hat{\tau} = -\epsilon_I \ln(1 - \beta e_I t/\epsilon_I)$ (Maflahi 2005). Hence the asymptotic matching shows that in fact, in the first two asymptotic stages, the three-step model can be reduced to a single step with the same form as the initiation step but which also releases the heat.

What happens subsequently in the three-step asymptotic structure depends on whether the adiabatic (final) explosion temperature T_{ad} is greater or less than T_B (Maflahi 2005). If $T_{\mathrm{ad}} < T_B$ then the branching rate remains exponentially small throughout and the asymptotic structure is identical to that of the one-step model given the above parameter matches (Blythe *et al.* 2005). In the case that $T_B < T_{\mathrm{ad}}$, the chain-branching rate comes into the leading-order balance once T reaches T_B and hence a small chain-branching explosion also occurs within an inner layer of the explosion region (J. Billingham, private communication), as is seen in figures 2(*d*) and 2(*e*).

However, the asymptotic solutions on which the parameter matching between the models is based are not quantitatively predictive for activation energies typically used in numerical calculations. Thus it remains to determine how the finite-activation-energy solutions agree between the one- and three-step models given this matching.

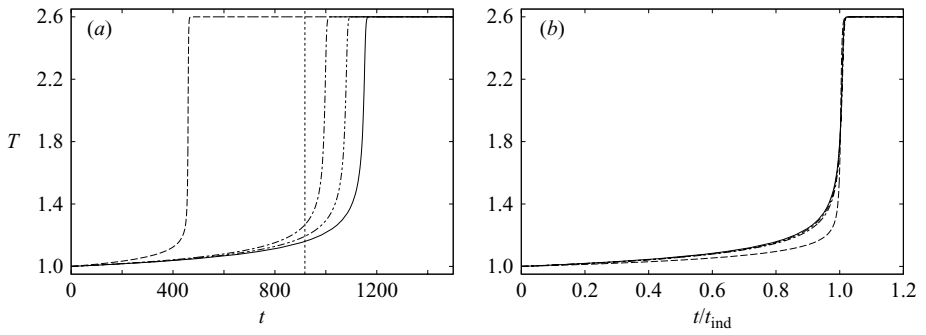

FIGURE 5. (*a*) Temperature histories for homogeneous explosion of the one-step model with $\epsilon = 1/15$ (solid line), and for the three-step model with $T_B = 1.2$ (dashed line), 1.9 (dot-dashed line) and 2.6 (double-dot-dashed line). (*b*) Same as (*a*) but with time rescaled such that $f = 0.5$ at unit time. Dotted line in (*a*) marks leading-order large-activation-energy induction time.

It also remains to determine what role T_B has in this regime of three-step solutions for finite activation energies.

Figure 5(*a*) shows the temperature in the homogeneous explosion for various values of $T_B > 1$, as well as for the one-step model when $\epsilon = \epsilon_I = 1/15$, which reveals that the three-step-model induction time is shorter than in the one-step model. However, as T_B is increased, the three-step homogeneous solution does rapidly converge to the finite-activation-energy one-step solution. Thus, given the parameter matches (3.19), for fixed finite $\epsilon = \epsilon_I$ the three-step model solution can be quantitatively described by the one-step model in the limit of large T_B. However, in figure 5(*b*), the time has been rescaled by the induction time, i.e. so that $f = 0.5$ at a time of unity in each case, and shows that even for more moderate values of T_B, the structures are virtually identical to the one-step solution on this time scale. Hence this indicates that even for finite activation energies, the three-step model can be effectively described by the one-step model with an activation energy which is precisely the chain-initiation activation energy, but where the definition of k^* in equations (3.19) needs to be modified to take into account the dependence of the induction time scale on T_B.

For the lowest value of the cross-over temperature ($T_B = 1.2$) shown in figure 5, the induction time is significantly shorter than the one-step value, and also than the asymptotic value (figure 5*a*), while the structure of the solution is also quantitatively different from the one-step solution (figure 5*b*): for $T_B = 1.2$, the induction zone is more weakly evolving, and the explosion region is thinner than for the one-step case. Hence, for this value of T_B, a one-step description of the three-step model is breaking down, and this is due to chain-branching effects becoming important as $T_B \to 1$. In other words, the one-step model only effectively describes the three-step model for values $T_B - 1 = O(1) > 0$, and becomes invalid as T_B approaches unity from above.

3.3. T_B near unity

When T_B approaches unity from above or below, figures 1 and 2 show that both thermal and chain-branching effects, and their competition, are important in the homogeneous explosion. Thus in these cases, all three steps of the model are important, and its solution cannot be effectively described by reduced models as for the $T_B - 1 = O(1)$ cases. Blythe *et al.* (2005) show that in the large-activation-energy asymptotic limit, this regime is in fact divided into three sub-regimes, $T_B = 1$, $T_B - 1 = O(\epsilon_B \ln \epsilon_B)$

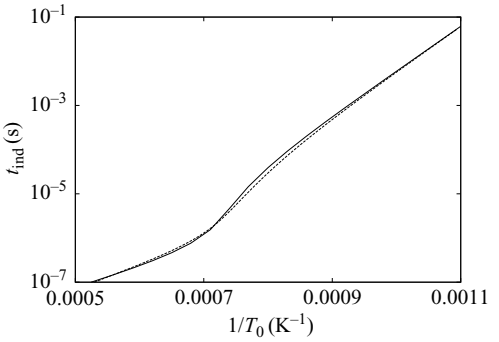

FIGURE 6. Induction time (logarithmic scale) of the homogeneous explosion against inverse initial temperature for hydrogen–air mixture at density 4.6 kg m^{-3}. Dotted line shows induction times from the three-step model with parameters fitted to the hydrogen data.

and $T_B - 1 = O(\epsilon_B)$, but that the asymptotic structures in each case do indeed show that the explosion region has both a thermal and chain-branching nature.

3.4. *Matching to detailed chemistry induction times*

From the above numerical and asymptotic results for the homogeneous explosion solutions of the three-step model, we now briefly show how the parameters of the model can be chosen in order to reproduce the constant-volume induction time data from detailed chemistry calculations. As an example, figure 6 shows the induction time as function of the initial temperature in an Arrhenius plot for stoichiometric hydrogen and air at a density of 4.6 kg m^{-3}, calculated using the method described in Radulescu (2003). Note that in this section, we will be dealing with dimensional versions of the parameters.

The data show two almost straight line regions (hence in which the induction time depends exponentially on $1/T_0$) joined by a narrow cross-over region around $1/T_0 = 0.0007$ K^{-1}. Thus the above results indicate that the relevant value of the cross-over temperature in the three-step model is $T_B = 1430$ K. Let us denote the straight line regions which exist for T_0 sufficiently above and below T_B as the lower and upper branches respectively. Since, according to the above asymptotic analysis for the three-step model, θ_B and θ_I are the effective activation temperatures when T_0 is sufficiently above or below T_B, respectively, their values are given by the slopes of the lower/upper branches in the Arrhenius plot. For the example shown in figure 6, this gives $\theta_B = 9300$ K and $\theta_I = 25000$ K. From the detailed chemistry calculations, the adiabatic temperature is $T_{\mathrm{ad}} \approx T_0 + 1900$ K. The rate constant k_C can then chosen so that the induction times on the lower branch are correct when the three-step model time scale is dimensionalized, and thence T_I is fixed by ensuring the induction time scale on the upper branch also matches the data. For our example, we obtain $k_C = 9.8 \times 10^6$ s^{-1}, $T_I = 2431$ K.

Figure 6 also shows the numerical induction times from the three-step model solutions when the above values of the parameters are used. It can be seen these three-step model results then do indeed match the data very well across the whole temperature range. The important point to note is that the results of the asymptotic study allowed us to chose the parameters of the model to match the data straightforwardly and uniquely without experimentation or multi-dimensional best fits. Note that for this example, choosing T_B as a reference temperature, we obtain the dimensionless values $\theta_B/T_B = 6.5$, $\theta_I/T_B = 17.6$, $(\gamma - 1)Q/T_B = 1.4$, $T_I/T_B = 1.7$.

The standard three-step model can similarly be fitted to induction time data of hydrocarbons such as acetylene which have similar features to those in hydrogen mixtures (Radulescu 2003). However, in this case one should take into account that the branching step may release significant heat (Varatharajan & Williams 2001), and hence how this alters the structures and asymptotic solutions when $T_B - 1 < 0$ needs to be examined. We intend to do so in the future. Other hydrocarbons, such as methane, do not show a cross-over effect in the induction time curves: their induction time appears to have single exponential dependence on $1/T_0$. Since in these mixtures the main reaction stage is very short compared to the induction zone, it could be argued that the three-step model can still be applied, but with a high value of T_B, such that the cross-over temperature is never reached. However, in such a case, the asymptotics above shows that the model could then be effectively reduced to a simpler one-step model.

4. Shock initiation

As in previous studies, here we consider one-dimensional shock initiation where the shock is produced by a constant-velocity piston moving in the x-direction, or equivalently by the reflection of a weaker shock from a stationary wall. For such a shock-induced ignition scenario, spatial dependence needs to be reinstated, and the governing equations are then

$$\left.\begin{gathered} \frac{\mathrm{D}\rho}{\mathrm{D}t} + \rho\frac{\partial u}{\partial x} = 0, \quad \rho\frac{\mathrm{D}u}{\mathrm{D}t} = -\frac{\partial p}{\partial x}, \quad \frac{\mathrm{D}e}{\mathrm{D}t} - \frac{p}{\rho^2}\frac{\mathrm{D}\rho}{\mathrm{D}t} = 0, \\ \frac{\mathrm{D}f}{\mathrm{D}t} = -R_I - R_B, \quad \frac{\mathrm{D}y}{\mathrm{D}t} = R_I + R_B - R_C, \end{gathered}\right\} \tag{4.1}$$

where u is the gas velocity in the x-direction, $p = \rho T$ is the pressure and $e = T/(\gamma - 1)$ is the internal energy. As usual, the results are given in the piston rest frame, i.e. such that x and u measure distance and speed with respect to the piston face. The pressure, temperature and density in (4.1) have been non-dimensionalized by using the values in the initial post-shock state, and velocity is then scaled with $\sqrt{\tilde{p}_s/\tilde{\rho}_s}$, so that distance is scaled with $\sqrt{\tilde{p}_s/\tilde{\rho}_s}/\tilde{k}_C$, where an '$s$' subscript denotes values in the initial post-shock state. The initial dimensionless shocked state is thus given by

$$p_s = 1, \quad \rho_s = 1, \quad T_s = 1, \quad u_s = 0, \quad f_s = 1, \quad y_s = 0. \tag{4.2}$$

If the initial shock Mach number is denoted by M_0, then the upstream, quiescent state (denoted by a zero subscript) is given by

$$\left.\begin{gathered} \rho_0 = \frac{\gamma - 1}{\gamma + 1} + \frac{2}{(\gamma + 1)M_0^2}, \quad p_0 = \frac{\gamma + 1}{\gamma + 1 + 2\gamma(M_0^2 - 1)}, \quad T_0 = p_0/\rho_0, \\ u_0 = (\rho_0 - 1)M_0\left(\frac{\gamma p_0}{\rho_0}\right)^{1/2}, \quad f_0 = 1, \quad y_0 = 0. \end{gathered}\right\} \tag{4.3}$$

Here we consider an initial shock Mach number $M_0 = 1.5$, together with the dimensionless parameter set (3.4), and vary T_B, which is now the ratio of the branching cross-over temperature to the initial shock temperature.

Equations (4.1) are solved using the second-order adaptive-mesh shock-capturing method described in Sharpe (2002) and Sharpe & Short (2004). The spatial resolution is chosen to ensure that the finest length scales which can appear in the problem are fully resolved (Maflahi 2004, 2005).

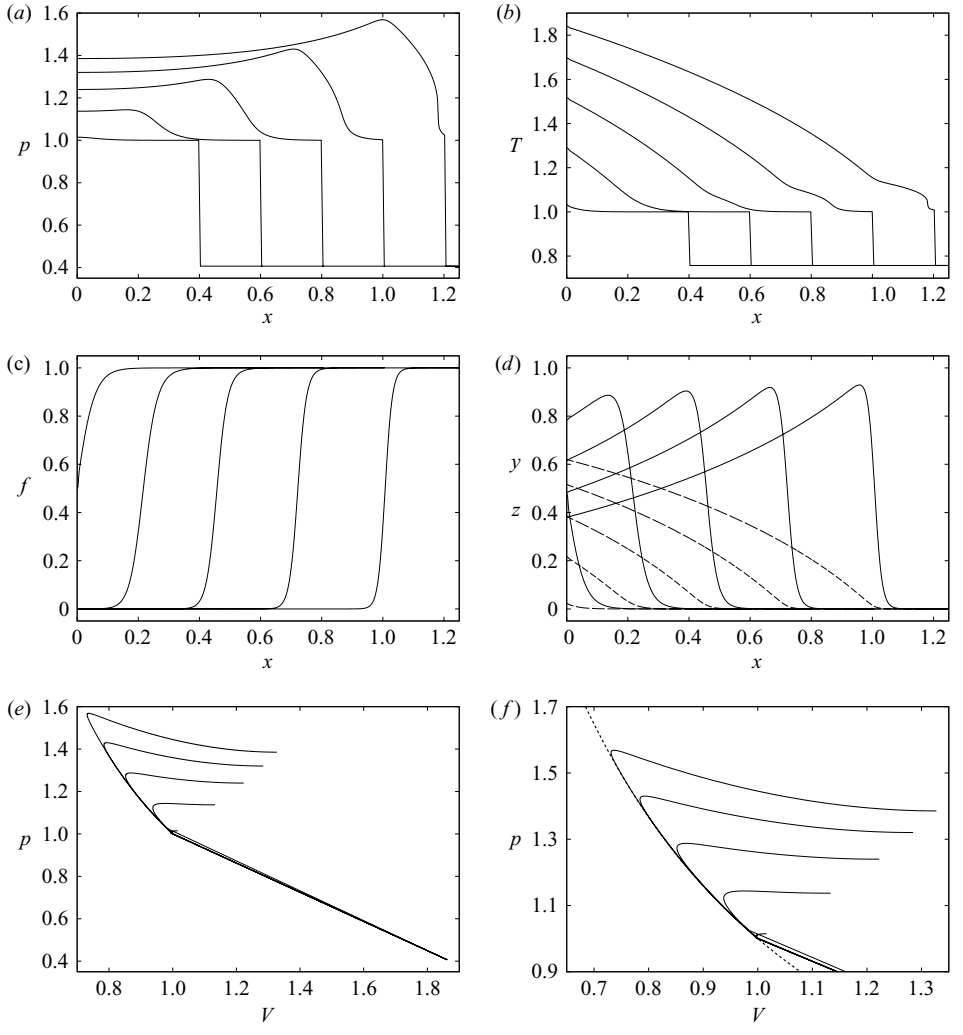

FIGURE 7. (*a*) Pressure profiles, (*b*) temperature profiles, (*c*) fuel mass fraction profiles, (*d*) radical (solid lines) and product (dashed lines) mass fraction profiles, (*e*) pV-diagrams and (*f*) pV-diagrams magnified in the region behind the shock (dotted line is the isentrope through the initial shock state), at times 0.483, 0.725, 0.966, 1.208 and 1.450. $T_B = 0.6$

4.1. *Results*

We first consider values of T_B in the regime $T_B - 1 = O(1) < 0$. As we have seen in § 3.1, the homogeneous-explosion solutions in this case have a explosion region which is mainly chain branching in nature, and the heat release in these solutions can be well described by the reduced two-step model. Of course, it does not necessarily follow that the two-step model can still quantitatively describe the three-step solutions for dynamic (spatially dependent) problems, such as shock initiation. Whether or not this is the case is examined below.

Figure 7 shows the evolution for the case $T_B = 0.6$, presenting spatial profiles of pressure, temperature and chemical mass fractions. Analogous to the homogeneous-explosion solution, initially there is a thermally neutral induction stage, and thus

there is no gas-dynamics between the piston and the shock, since the pressure and temperature remain virtually uniform. At $t = 0.483$ (the homogeneous-explosion induction time for this T_B), the chain-branching explosion begins at the piston, as can be seen in figures 7(*c*) and 7(*d*) which show rapid depletion of fuel and buildup of chain carriers near $x = 0$, with virtually no products having formed yet. The chain-branching explosion region (where f decreases rapidly and y increases to a maximum) can be seen to subsequently propagate away from the piston, since each particle reaches its induction time in turn as one moves away from the piston, due to the passage of the shock. Once the explosion is complete (which occurs first at the piston) the termination stage begins, producing heat and a build up of radicals. The heat release produces pressure disturbances, which begin to propagate away from the piston towards the shock at the sound speed of the undisturbed post-shock state.

The chain-branching explosion region can be shown to propagate away from the piston subsonically (Sharpe 2002; Dold & Kapila 1991). Indeed, the pressure and temperature disturbances created in the following exothermic termination region can be seen to move ahead of the branching region in figure 7. This results in an increasing pressure (as one moves back from the shock) part of the induction zone region. Figure 7(*a*) shows that subsequently a steepening front develops near the head of the disturbed induction region. By $t = 1.450$, the initial pressure disturbances have overtaken the shock, increasing its strength slightly, and the compressive front has steepened to the formation of a very weak secondary shock, although this steepened region collides with the shock before it has time to develop further.

The pV-diagrams in figures 7(*e*) and 7(*f*) clarify the evolution. In these diagrams, the profiles consist of the lead shock wave (which remains virtually undisturbed at the times shown), followed by the disturbed induction region, which has negative slope in the pV-plane, and which is in turn followed by a thin explosion region within which both the pressure and density reach a maximum. Subsequent to this, an expansive termination region in which the pressure and density decrease is apparent. One should not confuse the compressive disturbed induction zone region of the pV-diagrams with the exothermic reaction waves (weak detonations) associated with compressive pV-regions with negative slopes, as identified by Singh & Clarke (1992) and Clarke & Nikiforakis (1999). Indeed, ahead of the explosion region the reactions are not exothermic, hence here the energy equation can be replaced with the condition that the entropy is constant behind the shock, i.e. $p = 1/V^{\gamma}$ (since $p = V = 1$ just behind the undisturbed shock). Figure 7(*f*) shows that the disturbed induction zone region does indeed lie along $p = 1/V^{\gamma}$ (at least while the shock is not significantly disturbed by the overtaking pressure waves). Hence as particles pass through the induction zone, they evolve along the isentrope. This can also be shown to be the case for the two-step model results in Sharpe (2002). The exothermic termination region, which also lies along a negative slope in the pV diagrams, can however be identified with reaction-wave behaviour, and since it is expansive it is a fast flame (Singh & Clarke 1992; Clarke & Nikiforakis 1999). However, the slope of this region also has some curvature, indicating that it is an unsteady process (Clarke & Nikiforakis 1999). Furthermore, the magnitude of the slope of the termination region can be seen to increase with time in figure 7(*e*), and hence it is accelerating (Clarke & Nikiforakis 1999).

Subsequent to the times shown in figure 7 the compression wave overtakes the shock, resulting in a rapid strengthening of the shock front. The shock and termination zone then continue to accelerate, while the induction zone region becomes shorter due to higher post-shock temperatures. However, the fast-flame termination region accelerates faster than the shock, so that the final stage of the evolution is a smooth

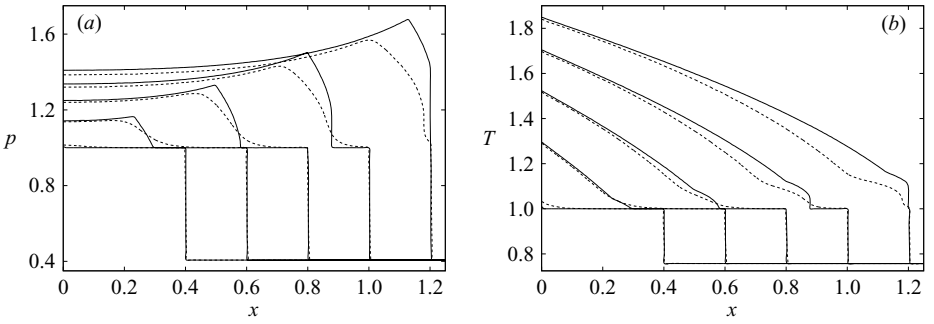

FIGURE 8. (*a*) Pressure profiles and (*b*) temperature profiles for the two-step model with $k = 0.476$ (corresponding to $T_B = 0.6$) at times 0.483, 0.725, 0.966, 1.208 and 1.450. Also shown as dotted lines are the three-step solutions with $T_B = 0.6$.

but slow growth of the shock–reaction complex into a fully coupled CJ detonation wave propagating through the quiescent explosive (Maflahi 2004).

This entire evolution for $T_B = 0.6$ is qualitatively like those described by the two-step model for values of k of order unity (for example it is intermediate between the $k = 5$ and $k = 0.25$ cases shown in Sharpe 2002). However, given the homogeneous-explosion parameter matchings between the two- and three-step model, it remains to determine how well the model solutions agree for the dynamical shock initiation scenario. For $T_B = 0.6$, the homogeneous explosion matching gives $k = 0.476$. Figure 8 shows the pressure and temperature profiles from a two-step model simulation with $k = 0.476$, at the same times as for $T_B = 0.6$ in figure 7 (these three-step solutions are also re-shown in figure 8 as dotted lines for direct comparison).

The results for the two models are in qualitatively good agreement, but there are noticeable differences. These differences are due to the assumption in the two-step model that the explosion is instantaneous and purely chain branching. In the full three-step model, however, while the main part of the explosion region is thin, the overall explosion zone scale is not negligible. For the homogeneous explosion, this is apparent from the analytical structure in equations (3.5) to (3.7). In particular, the induction and explosion regions both evolve on the same time scale, $e_B t$. For example, from figure 2(*a*) for $T_B = 0.6$ it can be seen that the time from which the explosion starts (when y reaches 0.01, say) to when it ends (when y peaks, say) is indeed comparable to the induction time. Even for $T_B = 0.6$, this finite explosion time still allows for a small degree of termination (and heat release) within it.

Returning to the shock initiation case, the replacement of the (spatially) distributed chain-branching explosion region in the three-step case by the instantaneous purely chain-branching explosion in the two-step model causes several differences from the three-step model solutions. The main difference is that the three-step model solutions appear as a 'diffused' version of the two-step solutions. For example, a difference can be seen in the point of maximum pressure that propagates away from the piston. In the two-step model, this is the point where $\xi(x, t) = 1$ and hence separates the induction stage ahead from the main reaction stage behind. Due to the switching on of the heat release at this point (via the Heaviside function in the main reaction step), the pressure and temperature gradients are discontinuous here. For the three-step case, however, because of the distributed explosion region, the pressure gradients are rapidly changing around the peak, but are nevertheless smooth.

The two-step model has another gradient discontinuity at the head of the disturbed induction zone region. This is the point which the sound wave from the first point of heat release has reached. This first disturbance occurred when the particle at the piston switched on its heat release stage (at the homogeneous induction time). Since the heat release was switched on instantaneously in the two-step model, this results in the gradient discontinuity at the lead sound wave from the termination zone. For the three-step model, however, since the termination rate begins in a more distributed fashion near the piston, as can be seen at the first time in the temperature plots in figure 8(*b*), the head of the disturbed induction zone region has a smooth structure. Indeed the initial heat release near the piston causes a 'foot' at the head of the disturbed induction zone at later times. It is this difference in the structures at the head of the disturbed induction region which causes the main difference between the solutions. In the two-step model, the flow profile steepens at the gradient discontinuity marking the head of the disturbed induction zone region. Indeed, by the third time shown in figure 8, a weak shock has formed here, which can be seen to then rapidly amplify as it propagates forward. At the last time shown in figure 8, this secondary shock is about to collide with the leading shock. For the three-step model however, the smoothed nature of the disturbed induction region results in a less rapid compressive steepening. In this case, the steepening forms behind the leading 'foot' region, but it only becomes a weak shock just before it collides with the lead shock.

Despite these differences, the two-step solutions are still sufficiently representative of those of the three-step model that the two-step studies in Sharpe (2002) should provide useful predictions of how the evolution will depend on T_B (via k). For the two-step model, the evolution is sensitive to k, and hence it will be sensitive to T_B in the three-step case. In particular, the results in Sharpe (2002) predict that, for increasing T_B, corresponding to increasing k, the secondary shock will form closer to the piston and have more time to amplify before it collides with the leading shock. On the other hand, Sharpe (2002) predicts that for sufficiently low T_B, corresponding to small values of k, no secondary shock will form and instead the pressure disturbances couple directly with the leading shock.

These predictions of the dependence of the solution on T_B from the two-step study are confirmed in figures 9 and 10, which shows the evolution for $T_B = 0.5$ and $T_B = 0.8$ ($k = 0.101$ and 3.22, respectively). In the case of $T_B = 0.5$, it can be seen that heat release at the piston begins when the shock has moved a smaller distance than for $T_B = 0.6$, and the disturbances reach and couple with the shock before any significant steepening can occur, as predicted. For the larger value of $T_B = 0.8$, figure 10 shows that since now the induction time is of the order of the termination-rate time scale, the shock has moved quite far by the time that heat release begins at the piston, and hence the compressive induction zone region does have time to steepen significantly, and a secondary shock forms long before the disturbances catch up with the leading shock. However, unlike the two-step case, where the secondary shock always forms at the head of the disturbed region, in this three-step case the shock forms inside the smoothed disturbed induction zone region.

However, it should be noted that for $T_B = 0.8$, as in the homogeneous explosion, the assumptions of the two-step model are breaking down. This is because there is now a significant overlap of branching and termination within the explosion region. For example, at the first time shown in figure 10, both radicals and a smaller amount of products can be seen to be building up in a region near the piston. This build up of products results in a small but significant temperature gradient nearer the piston (figure 10*b*), even before the homogeneous induction time. Indeed, the explosion region

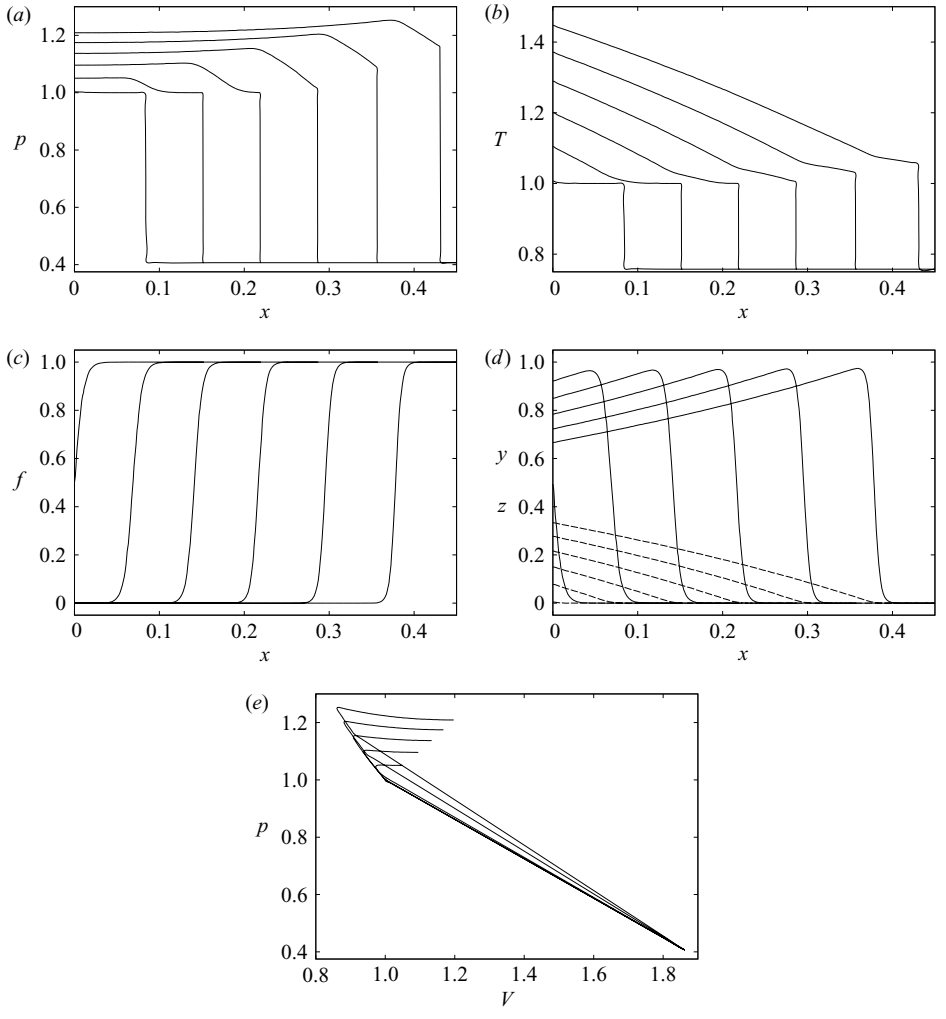

FIGURE 9. (*a*) Pressure profiles, (*b*) temperature profiles, (*c*) fuel mass fraction profiles, (*d*) radical (solid lines) and product (dashed lines) mass fraction profiles and (*e*) pV-diagrams, at times 0.101, 0.183, 0.263, 0.345, 0.426 and 0.507. $T_B = 0.5$.

which propagates away from the piston is now initially quite thick, e.g. occurring over a distance of order unity around the pressure maximum at the second and third times shown in figure 10. Nevertheless, the explosion region still propagates subsonically, in qualitative agreement with the two-step predictions, since disturbances can be seen to propagate ahead of the explosion region into the induction zone. The pV-diagrams show that while the initial part of the disturbed induction region (as one moves back from the shock) still lies along an isentrope, there is now a significant compressive region where the pV-curve departs from the isentrope before the pressure maximum is reached. Again, this is due to small but significant heat release occurring in the thick explosion region before the pressure maximum. The main part of the termination stage is still an expansive fast-flame region in the pV-diagram.

As the secondary shock forms and amplifies, due to the increasing temperatures behind it, the following explosion region becomes thinner. This is due to the post-shock

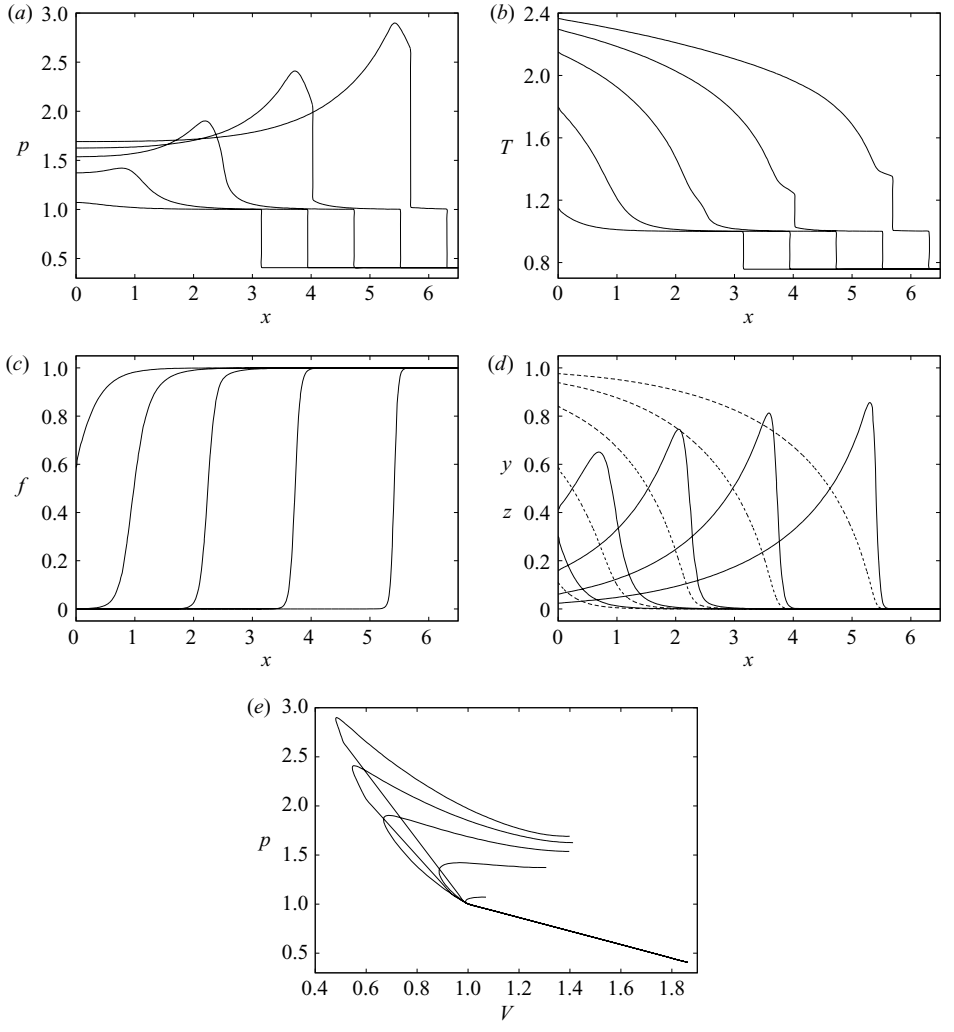

FIGURE 10. As figure 9 but at times 3.801, 4.752, 5.702, 6.652 and 7.602. $T_B = 0.8$.

temperatures becoming increasingly above the chain-branching crossover temperature, resulting in the chain-branching rate increasing exponentially rapidly behind the shock. This can be seen in figure 10(*d*), where the peak radicals increases with time, and the overlap between the branching and termination stages decreases, so that the explosion region is becoming more purely chain branching in nature. The last two times in the pV diagrams show that both the shock and fast-flame termination region are accelerating (since their slopes are increasing in figure 10*e*). However, they do not accelerate rapidly enough to even begin to approach a full coupling into a strong CJ detonation (at which point they would lie along a common line in the pV-plane) before the shocks collide. Subsequently, the shock collision rapidly produces a strong detonation propagating through the quiescent fuel.

We next consider solutions for the values of $T_B > 1$. As we have seen in § 3.2, the homogeneous explosions for such values are mainly thermal, and can be effectively described by the reduced one-step model. Again, it remains to examine whether this is still the case for the shock-initiation scenario.

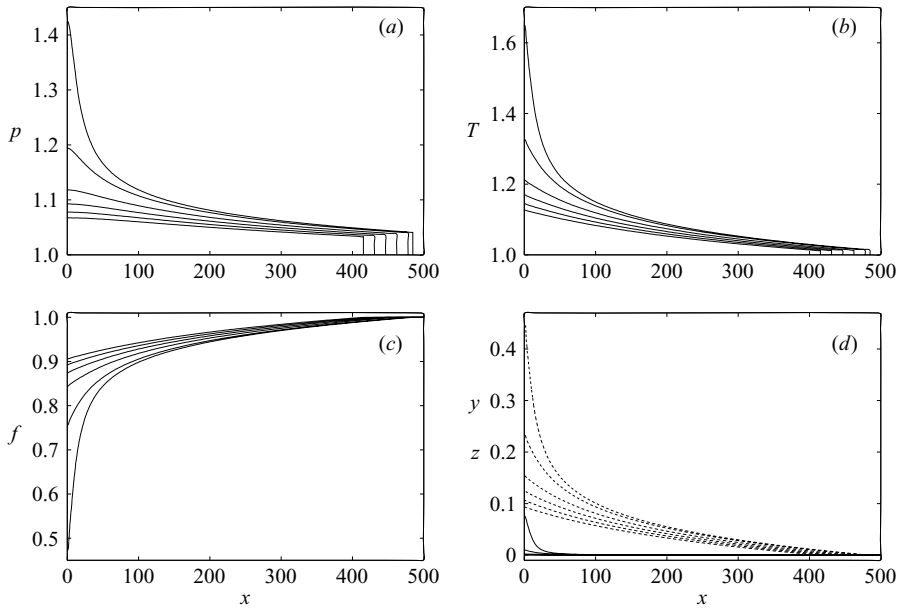

FIGURE 11. (*a*) Pressure profiles, (*b*) temperature profiles, (*c*) fuel mass fraction profiles, and (*d*) radical (solid lines) and product (dashed lines) mass fraction profiles, at times 494.4, 512.7, 531.0, 549.3, 567.6 and 575.4. $T_B = 1.2$.

Sharpe & Short (2004) show the complete one-step evolution in their figures 5, 9 and 10 for the same parameters as used here ($Q = 4$, $\gamma = 1.4$, $M_0 = 1.5$, $k^* = k_I$ and $\epsilon = \epsilon_I = 1/15$). Note that Sharpe & Short (2004) used the high-activation-energy asymptotic induction time to non-dimensionalize time, and hence their distance and time-scales need to be multiplied by 917.8 in order to obtain the scales used in this paper, given the homogeneous explosion parameter matching (3.19). To summarize their results briefly here, a reaction wave emerges at $t = 1390$, which largely consists of a (shockless, supersonic) weak detonation, followed by an unsteady region and very small fast-flame region, which only occur in the region where $z = 1 - f$ is less than about 0.2. The unsteady region moves forward through the reaction wave as it propagates, but a secondary shock forms at $t = 1436$, $x = 165$, at a point inside the reaction zone where $z \approx 0.6$. The shock and reaction zone then rapidly couple into a strong detonation propagating though the shocked material by about $t = 1520$, $x = 410$.

Figures 11 and 12 show the evolution for the three-step model with $T_B = 1.2$. Figure 11 shows the evolution during the initial induction stage. As in the homogeneous explosion in this case, radicals produced by the initiation step are rapidly converted directly into products and heat by the termination step, with the amount of radicals initially remaining virtually zero everywhere. In the shock-initiation case, since the material nearer the piston has been shocked (hence releasing heat) longer than that nearer the shock, this produces gas-dynamical evolution, which results in a weak gradient in pressure and temperature, just as for the one-step model solutions. The heat release also produces a very weak increase in the shock strength (cf. Sharpe & Short 2004). Only once thermal runaway begins at the piston at $t = 575$, and the temperature approaches T_B there, does a small degree of chain branching begin to occur (figure 11*d*), analogous to the homogeneous explosion.

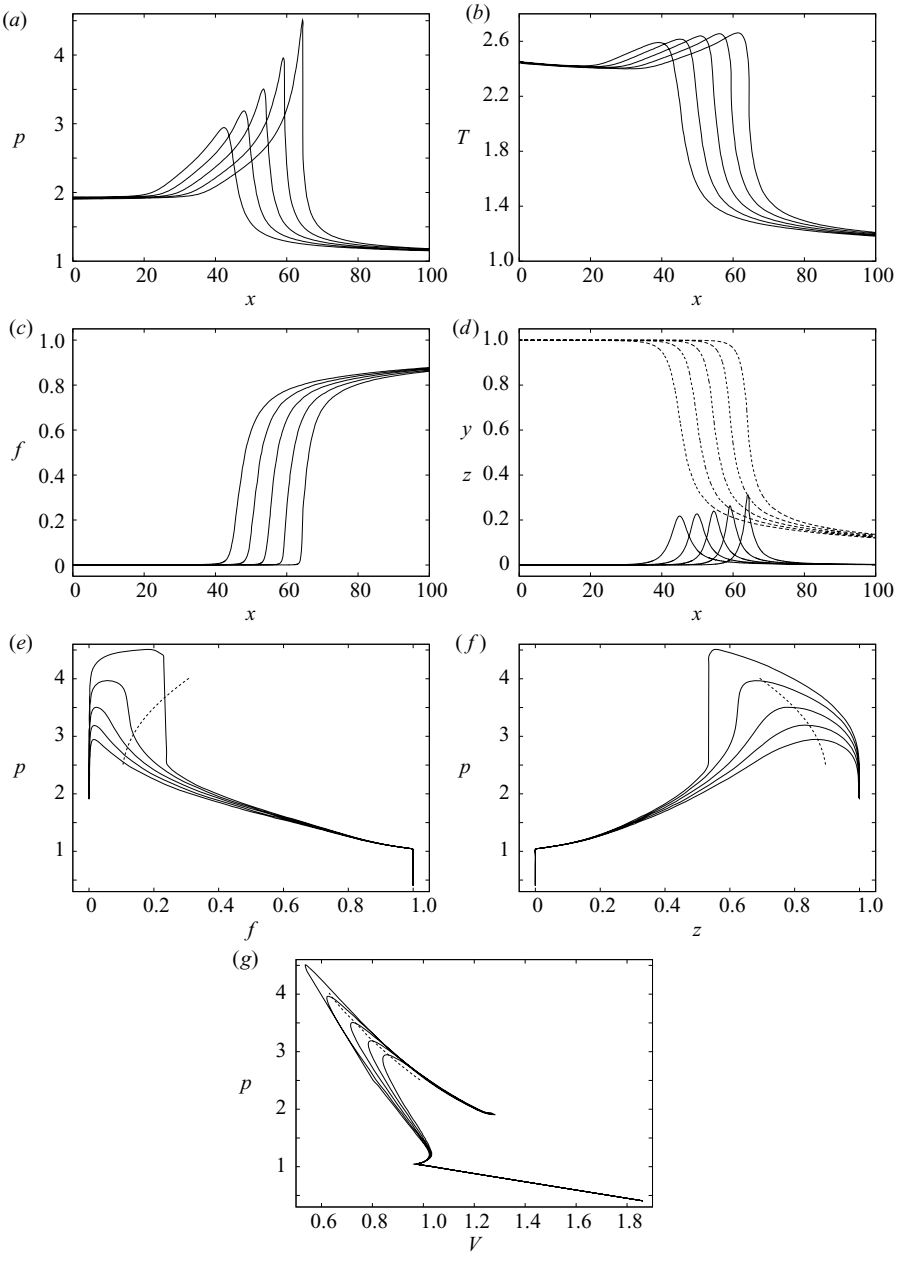

FIGURE 12. (*a*) Pressure profiles, (*b*) temperature profiles, (*c*) fuel mass fraction profiles, (*d*) radical (solid lines) and product (dashed lines) mass fraction profiles (all profiles shown in a post-leading-shock region), (*e*) pf-diagrams, (*f*) pz-diagrams and (*g*) pV-diagrams, at times 590.5, 592.3, 594.1, 596.0 and 597.8. $T_B = 1.2$. Dotted lines are loci of the pressure maximum from the one-step model solutions.

Subsequent to the explosion at the piston, a forward moving reaction wave emerges as particles further from the piston subsequently explode in turn. In this case, the reaction wave emerges at around $t = 580$, much earlier than for the one-step case, as expected from the homogeneous result in figure 5. Figure 12 shows the initial

evolution after the emergence of the reaction wave. At this stage, starting at the shock and moving back to the piston, the solution consists of an induction region through which pressure and temperature increase and the fuel fraction decreases (the product fraction increases), which is then followed by a rapid, but smooth, increase of the pressure to a maximum. The pV-diagrams in figure 12(g) reveal that, since this compressive reaction wave lies mostly along a straight line with negative slope, it is in fact part of a supersonic weak detonation, and it is decelerating since the slope decreases with time (Clarke & Nikiforakis 1999). Figure 12(g) also shows that the region around the pressure maximum is highly curved in the pV-diagrams and hence this is an unsteady region. This unsteady region is in turn followed by an expansion wave.

Figures 12(e) and 12(f) show the solutions in pressure–fuel fraction and pressure–product fraction planes, which help to reveal where various features lie within the reaction zone. The pf-diagrams show that, initially, the fuel is depleted within the weak detonation: the pressure increases as f decreases and the pressure maximum occurs only once f is nearly zero. Hence, as can predicted by the differences in the homogeneous structures in figure 5(b) (Sharpe & Short 2004), for $T_B = 1.2$ the weak detonation consists more nearly of the entire explosion region than for the one-step model. Indeed, figure 12(e) also shows as a dotted line the locus of the pressure maximum in the pf-plane (which is a rough measure of the end of the weak detonation part of the reaction wave) for the one-step model solution. As can be seen, for $T_B = 1.2$, the rear of the weak detonation lies significantly further towards the completely burnt fuel state, $f = 0$, than for the one-step model.

Figure 12(d) shows that the nature of the reactions in the weak detonation in the three-step solution is different to that of the purely thermal one-step model, in that a moderate, but increasing, amount of chain branching occurs within the weak detonation. Indeed, it is also important to note that for the homogeneous explosion with $T_B = 1.2$ shown in figure 5, the validity of the one-step description is beginning to break down, since chain-branching effects in the explosion are becoming significant. The maximum in the radical mass fraction occurs within the explosion region, before the pressure maximum is reached. After the fuel is completely depleted, a small but significant amount of radicals still exists, and hence the heat release is not completed within the explosion region, unlike in the one-step model case. Instead, there is small following termination region in which the radicals are depleted. This can be seen best in the pz-diagram in figure 12(f), which shows that, although the fuel is almost completely depleted there, the pressure maximum occurs while the composition is still not all products. Thus the unsteady region around the pressure maximum is a combustion region in which heat is still being released. This region moves forward away from the end of the reaction zone in figure 12(f), so that the final part of the heat release then begins to occur within the expansive region, which can be identified as part of a quasi-steady fast flame from the pV-diagrams (Clarke & Nikiforakis 1999; Singh & Clarke 1992). The pz-diagrams, which show the structure of the complete exothermic reaction zone, rather than just the explosion region as in the pf-diagrams, are in fact remarkably similar to the pz-diagrams for the one-step solutions in Sharpe & Short (2004). Thus, for the purpose of a more direct measure of comparison, the locus of the pressure maximum from the one-step calculations is also shown in figure 12(f). This can be seen to be in quantitative agreement with the $T_B = 1.2$ three-step model solution. Similarly, the pV-evolution in figure 12(g) is also in quantitative agreement with that for the one-step solution (again, the locus of the pressure maximum from the one-step calculation is also shown). The pressure

and temperature profiles in figures 12(*a*) and 12(*b*), are also in qualitative agreement with the results in Sharpe & Short (2004), although the time and distance scales are markedly different, which is to be expected given the difference in the homogeneous induction times on the termination time scale.

By the final time shown in figure 12, a secondary shock has formed and begun to amplify and move through the weak detonation ahead of it, transforming it into a following fast flame. The shock forms at about $t = 597$, $x = 62$, which is much earlier and closer to the piston than for the one-step results in Sharpe & Short (2004) on the time scale used here. However, figure 12(f) shows that the secondary shock forms when $z \approx 0.6$, again in quantitative agreement with the shock formation point in the one-step model. It is important to note that, for the one-step model, different shock initiation solutions are classified according to how the solutions evolve in the pV- and pz-diagrams, and for the three-step model these are found to be insensitive to T_B as it is increased. Hence in these terms, the evolutionary mechanisms of the three-step gas-dynamical evolution are very well predicted by the one-step model (which represents the three-step model in the limit of large T_B) even when T_B is as low as 1.2. While the timings differ considerably on the termination-rate time scale, as T_B increases, these times also rapidly tend to those of the one-step model. In summary, it appears that, while the one-step model cannot describe the details of the chemistry, it does effectively capture the way in which the heat release and gas-dynamics couple in the three-step model even for $T_B = 1.2$, at least up to the point of secondary shock formation.

However, once the secondary shock has formed, it then rapidly amplifies. If the secondary shock temperature subsequently reaches and exceeds T_B, then chain branching will become dominant over chain termination in the reaction zone behind the secondary shock. Hence at this point, the evolution may be expected to become quantitatively different to that in the one-step model. Figure 13 shows the evolution subsequent to the secondary shock formation for $T_B = 1.2$. The rapid growth of the shock as it propagates through the disturbed induction region behind the leading shock can be seen. Figure 13(*d*) shows that chain branching does indeed rapidly become more dominant in the following reaction zone. As the secondary shock temperature increases, the remaining part of the induction zone behind it becomes shorter and the subsequent explosion becomes more chain branching in nature, as can be seen by the increasing radical peak and the overlap with the following termination stage becoming less pronounced.

The loci of the maximum pressure (which occurs at the secondary shock) in the one-step model solution is also shown for direct comparison in figure 13(*e*–*g*). As expected, the three-step solution does become quantitatively different from that of the one-step model at this stage. In particular, the shock accelerates through the partially reacted material ahead of it more quickly in the three-step case. This can be seen from figure 13(f), which shows that when the maximum (secondary shock) pressure has reached a given value, the shocked material is less burnt (z is smaller) in the three-step case compared to the one-step solution. Furthermore, for a given value of the maximum pressure, the pressure just ahead of the secondary shock is slightly lower in the three-step case than in the one-step case. Thus the secondary shock evolves to a strong detonation along different loci in the pV-plane (figure 13g).

Despite these differences, the pV-, pf- and pz-diagrams in figure 13 show that this stage of the evolution is still in very good qualitative agreement with the one-step solutions. In particular, in both cases the secondary shock very rapidly accelerates through the remaining portion of the weak detonation ahead of it, converting the

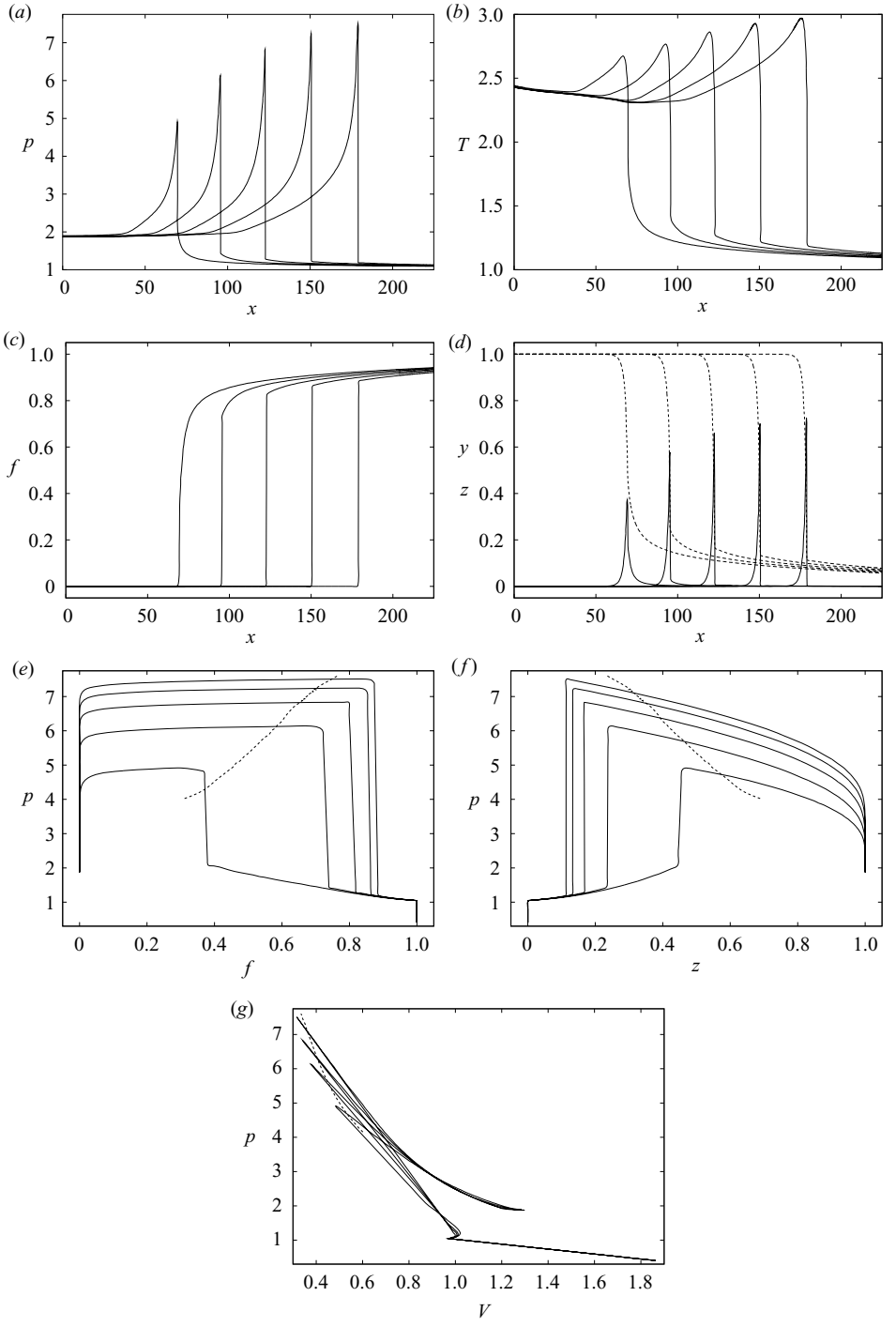

FIGURE 13. As figure 12 but at times 599.7, 608.8, 618.0, 627.1 and 636.3 (pV-diagram not shown at $t = 627.1$ for clarity). $T_B = 1.2$.

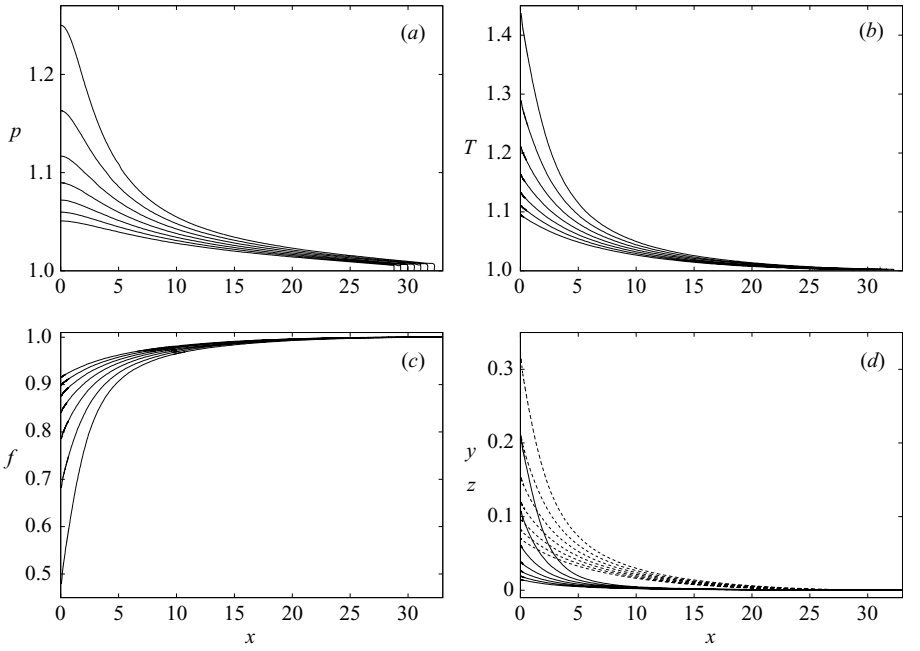

FIGURE 14. (*a*) Pressure profiles, (*b*) temperature profiles, (*c*) fuel mass fraction profiles, (*d*) radical (solid lines) and product (dashed lines) mass fraction profiles at times 34.6, 35.3, 36.0, 36.7, 37.4, 38.1 and 38.8. $T_B = 1.0$.

weak detonation into a quasi-steady fast flame behind it. The shock thus moves into a less and less burnt state, i.e. $f \to 1$, $z \to 0$ at the shock. Also, the fast flame accelerates with the shock (its slope increases in the pV-plane), but faster than the shock, such that they couple into a fully formed strong detonation (they begin to lie along a common straight line in the pV-plane), for both models. As T_B is increased, this stage of the evolution also becomes in better quantitative agreement with the one-step model solutions.

The remaining cases left to consider are those in which T_B is close to unity. In these cases, it is expected from the homogeneous explosion that both chain branching and termination effects will be important from the outset, and that the explosion region which emerges from the piston will have a mixed chain-branching/thermal nature. However, it is unclear at this stage whether this explosion will propagate away from the piston subsonically as for $T_B - 1 = O(1) < 0$ or supersonically as for $T_B - 1 = O(1) > 0$.

Figures 14 and 15 show the shock-induced ignition evolution when $T_B = 1$. The initial induction stage evolution is shown in figure 14. At this stage, the initiation step slowly produces radicals which leads to both branching and termination. Initially, analogous to the homogeneous explosion structure in figure 2, termination is somewhat more dominant in the induction zone, with more products being produced at a given spatial position than radicals. However, as the time of explosion at the piston face is approached and the temperature begins to rapidly increase, radicals begin to build up more rapidly there. Note that, again similar to the homogeneous-explosion solutions, the explosion at the piston occurs much earlier than for $T_B = 1.2$ ($t = 39$ as compared to $t = 575$). However, even taking into account this difference in timings by rescaling the time and length scales using the homogeneous induction

times in both cases (e.g. as was done in figure 5*b*), a number of differences in the induction stage solutions prior to the explosion at the piston are apparent when comparing figure 14 with figure 11 for $T_B = 1.2$,

These differences are due to the fact that a significant amount of radicals is produced in the induction stage for $T_B = 1.0$ (as compared to almost none in the $T_B = 1.2$ case) and hence less heat is produced by the competing termination step for a given amount of consumption of the fuel, i.e. the induction stage is less thermal for $T_B = 1.0$. First, this results in the pressures and temperatures at the piston being lower for $T_B = 1.0$ when f has reached a given value there. Secondly, again analogous to the differences in the homogeneous-explosion solution structures, this results in the temperature gradient behind the shock being much smaller for $T_B = 1.0$, and also in a smaller increase in the leading shock strength by the time of explosion at the piston. Indeed, for a given value of f at the piston, the fuel fraction profiles for $T_B = 1.0$ are initially much more weakly decreasing as one moves back from the shock than for $T_B = 1.2$, but in both cases f then decreases rapidly in a region close to the piston face as the explosion time there is approached. Finally, although in both cases the gas-dynamical evolution delays the explosion at the piston compared to the homogeneous explosion induction time, the delay is smaller for $T_B = 1.0$ ($f = 0.5$ at the piston occurs at a time 12% later than the homogeneous explosion time for $T_B = 1.0$, compared to a time 22% later for $T_B = 1.2$).

Figure 15 shows the emergence of the reaction wave and the subsequent evolution. The pV-diagrams (figure 15*g*) show that, as for larger T_B values and the one-step model, the lead part of the reaction wave initially propagates at infinite speed, since the slope is vertical at the first time shown (Clarke & Nikiforakis 1999). This compressive part of the reaction wave is therefore a weak detonation, and it rapidly decelerates since its slope decreases in the pV-plane. The pf-diagrams in figure 15(*e*) show that as for the $T_B = 1.2$ case, this weak detonation part of the wave occurs within the explosion region, since the pressure maximum initially occurs only once f is close to zero. However, now there is a significant amount of chain branching within the weak detonation. The radical peak seen in figure 15(*d*) occurs ahead of the pressure maximum, and this peak also increases with time as the temperatures reached within the explosion region increase. There is thus a significant termination region after the explosion region, in which the radicals are converted into products and heat. This can be more clearly seen in the pz-diagrams (figure 15*f*). For $T_B = 1.0$ the pressure maximum initially occurs at around $z = 0.5$, i.e. when the composition is significantly further from being all products than for $T_B = 1.2$. The pf- and pV-diagrams hence show that now only a small part of the complete exothermic reaction zone consists of the weak detonation region, with the majority occurring in the unsteady combustion region and a following quasi-steady fast-flame part. The pressure maximum moves forward as the compressive region ahead of it steepens, until a secondary shock forms at about $x = 9$, at a point inside the reaction zone where $z \approx 0.17$. Hence the secondary shock forms much further towards the front of the reaction wave than for $T_B = 1.2$ or in the one-step model solution.

Another difference between the $T_B = 1.0$ results and those for higher values is that for $T_B = 1.2$ and the one-step model, the weak detonation propagates through an unsteady induction zone region. This unsteady induction zone is represented by the regions of positive slope which occur just after the leading shock in the pV-diagrams of figure 12(*g*) and in figure 5 of Sharpe & Short (2004). For $T_B = 1.0$, however, the unsteady induction region is much diminished. Indeed, in figure 15(*g*), the weak detonation begins virtually at the post-shock state. Thus in this case, the weak

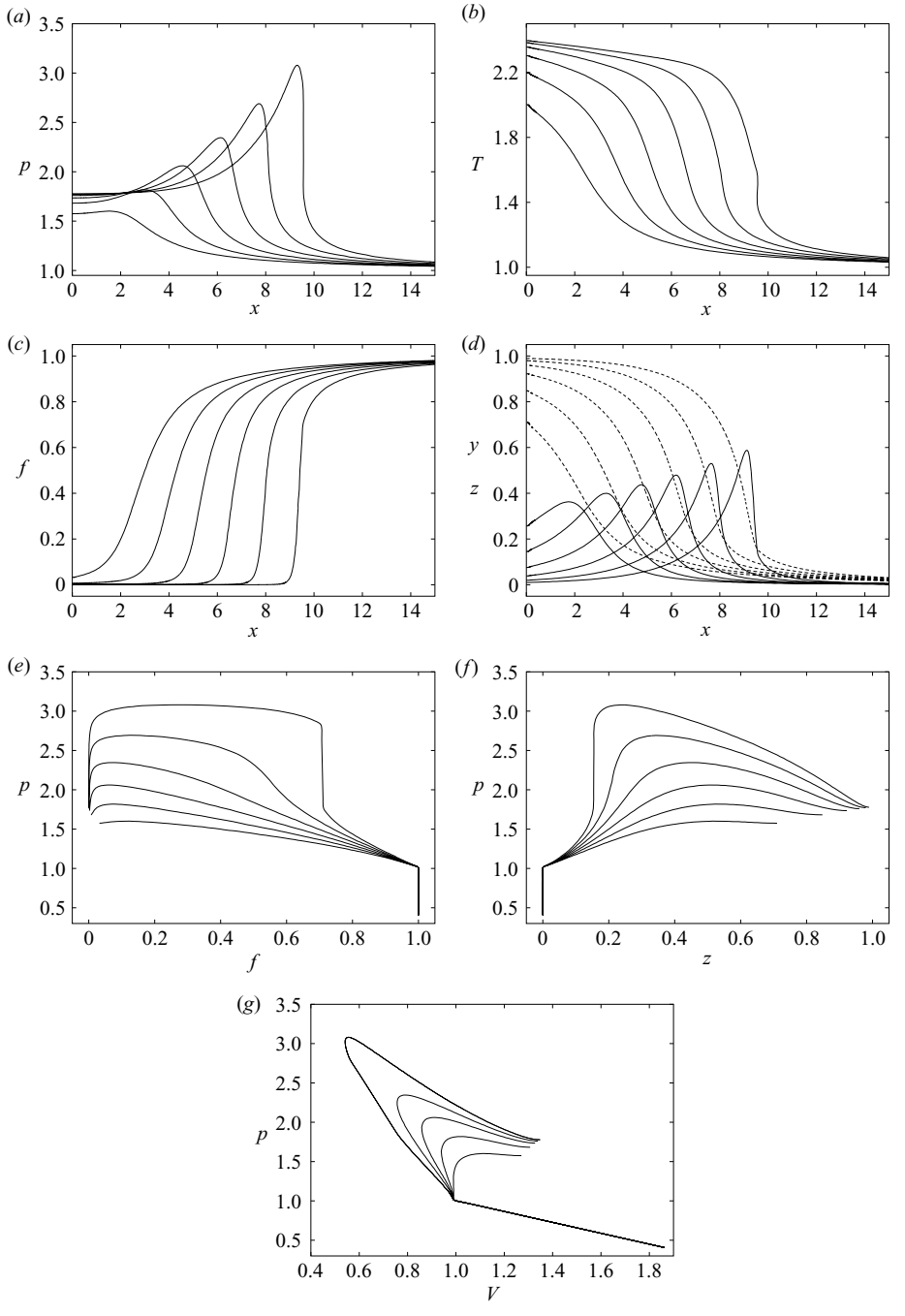

FIGURE 15. (*a*) Pressure profiles, (*b*) temperature profiles, (*c*) fuel mass fraction profiles, (*d*) radical (solid lines) and product (dashed lines) mass fraction profiles (all profiles shown in a post-leading-shock region), (*e*) pf-diagrams, (*f*) pz-diagrams and (*g*) pV-diagrams, at times 40.2, 40.9, 41.6, 42.3, 43.0, 43.7. $T_B = 1.0$.

detonation propagates through a much more uniform region than in the larger T_B cases. This is due to the much weaker evolution of the temperature/pressure gradients behind the shock in the induction stage of the evolution for $T_B = 1.0$.

The $T_B = 1.0$ evolution, with the smaller weak detonation part of the reaction zone and the secondary shock forming nearer the front of the reaction wave, is in fact reminiscent of one-step solutions when a lower value of ϵ is used (Sharpe & Short 2004). However, there is a major difference, in that the reaction wave evolution occurs much further behind the leading shock for the $T_B = 1.0$ case than for the less temperature sensitive one-step model solutions. The result is that, once the secondary shock forms in the three-step model, it strengthens sufficiently to reach a fully developed strong detonation before it collides with the leading shock, while in the lower ϵ one-step results, the secondary shock forms quite near the leading shock, and does not have time to strengthen significantly before the shocks collide (cf. the $\epsilon = 1/10$ case in figure 7 of Sharpe & Short 2004).

5. Conclusions

Both spatially homogeneous explosion and initiation of reactive materials by a shock wave have been investigated using a standard three-step chain-branching chemistry model. For homogeneous explosions, it was shown that the three-step model can be effectively described by the widely used simpler (reduced) one-step and two-step models, provided the ratio of the chain-branching cross-over temperature to the initial temperature, T_B, is within certain regimes. The two-step model, which assumes a purely chain-branching explosion region, is valid provided T_B is sufficiently below unity, while the purely thermal one-step model can effectively describe the three-step homogeneous explosion solutions provided T_B is sufficiently greater than unity. When T_B is close to unity, all the reaction steps in the three-step model are important, and hence the solutions cannot be described by a reduced model. Furthermore, in the relevant regimes, it was shown how the parameters of the reduced one-step or two-step models are related to those of the three-step model in order to obtain a match of the homogeneous explosion structures. This parameter identification helps to reveal the crucial role of the cross-over temperature in chain-branching chemistry, in that not only does the reaction structure change dramatically as T_B is varied around unity, but also the effective activation energy changes from that of the chain-branching step to that of the initiation step as T_B is increased through unity. Hence the temperature sensitivity of the reaction also changes dramatically.

In the shock initiation scenario, for an initial shock temperature sufficiently above the branching cross-over temperature, the three-step model results are in qualitative agreement with those of the two-step model. For example, the chain-branching explosion region is found to propagate away from the piston subsonically, so that disturbances from the exothermic termination region propagate ahead of the explosion into the induction zone. Also in agreement with the two-step model predictions, a secondary shock only forms if T_B is sufficiently large, otherwise the exothermic region couples directly with the leading shock. However, unlike the homogeneous-explosion scenario, the three-step solutions are not in quantitative agreement with those of the two-step model. The two-step model underpredicts the value of T_B at which secondary shock formation first occurs, and also the spatial position where the secondary shock forms in the solution, if it does occur. These differences are due to the invalidity of the assumption in the two-step model that the explosion region occurs instantaneously and is purely chain-branching in character. Furthermore, the long thermally neutral

induction zone regimes considered in previous studies using the two-step model are found to be unachievable in the context of the three-step model.

For an initial shock temperature sufficiently below the chain-branching cross-over temperature, as predicted by the homogeneous explosion study, it is found that the one-step reaction model effectively captures the way the heat release couples with the gas-dynamics in the three-step model. In particular, in agreement with the previous one-step model studies, the evolution begins with a thermal induction stage, subsequent to which a supersonic but decelerating reaction wave emerges. The length and time scales over which the evolution occurs decreases with T_B, but even for T_B only moderately above unity, the evolutionary mechanisms are found to be described well by the one-step model, in terms of the composition of the reaction wave as weak detonation, unsteady combustion, and fast-flame parts.

For initial shock temperatures closer to the branching cross-over temperature, both chain-branching and thermal effects, and the competition between them, are important from the outset. As T_B is increased to unity from below, the speed at which the explosion region emerges from the piston face changes from subsonic to supersonic. For T_B equal to or just above unity it was found that the reaction wave emerges with an initially infinite speed but rapidly decelerates, as in the one-step model, and hence the wave begins as a weak detonation. However, new behaviour is observed for the three-step model, in that a significant amount of chain branching occurs within the weak detonation part of the reaction wave. As T_B is decreased towards unity, the portion of the reaction wave which consists of the weak detonation part shrinks, and the secondary shock forms closer to the front of the wave. This dependence on T_B is somewhat like the effect of decreasing the activation energy in the one-step model.

G. J. S. was in receipt of an EPSRC Advanced Fellowship during the course of this work, and N. M. was funded through an EPSRC Doctoral Training Account. The authors are also grateful to John Billingham and Matei Radulescu for useful discussions, and to Mantis Numerics Ltd for the provision of the numerical code, Cobra, used to perform the simulations in this paper.

REFERENCES

Blythe, P. A. & Crighton, D. G. 1989 Shock-generated ignition: the induction zone. *Proc. R. Soc. Lond.* A **426**, 189–209.

Blythe, P. A., Kapila, A. K. & Short, M. 2005 Homogeneous ignition for a three-step chain-branching reaction model. *J. Engng Maths* (submitted).

Clarke, J. F. & Nikiforakis, N. N. 1999 Remarks on diffusionless combustion. *Phil. Trans. R. Soc. Lond.* A **357**, 3605–3620.

Dold, J. W. & Kapila, A. K. 1991 Comparison between shock initiations of detonation using thermally-sensitive and chain-branching chemical models. *Combust. Flame* **85**, 185–194.

Gustavsen, S. A., Sheffield, S. A., Alcon, R. R. & Hill, L. G. 2002 Shock initiation of new and aged PBX 9501. *Los Alamos National Laboratory Rep.* LA-UR-02-3651.

Jackson, T. L. & Kapila, A. K. 1985 Shock induced thermal runaway. *SIAM J. Appl. Maths* **45**, 130–137.

Kapila, A. K. 1983 *Asymptotic Treatment of Chemically Reacting Systems*. Pitman, Boston.

Kapila, A. K. & Dold, J. W. 1989 A theoretical picture of shock-to-detonation transition in a homogeneous explosive. In *9th Intl Symp. on Detonation*, pp. 219–227. Office of Naval Research Arlington.

Maflahi, N. 2004 Theory of explosions and detonations for a three-step chain-branching chemistry model. MPhil(Sci,Qual) thesis, University of Birmingham, Birmingham, UK.

Maflahi, N. 2005 Theory of explosions and detonations for a three-step chain-branching chemistry model. PhD thesis, University of Birmingham, Birmingham, UK.

Meyer, J. W. & Oppenheim, A. K. 1971 On the shock-induced ignition of explosive gases. *Proc. Combust. Inst.* **13**, 1153–1164.

Ng, H. D. & Lee, J. H. S. 2003 Direct initiation of detonation with a multi-step reaction scheme. *J. Fluid Mech.* **476**, 179–211.

Nikiforakis, N. & Clarke, J. F. 1996 Numerical studies of the evolution of detonations. *Math. Comput. Model.* **24**, 149–164.

Radulescu, M. I. 2003 The propagation and failure mechanism of gaseous detonations: experiments in porous-walled tubes. PhD thesis, McGill University, Montreal, Canada.

Sharpe, G. J. 2002 Shock-induced ignition for a two-step chain-branching kinetics model. *Phys. Fluids* **14**, 4372–4388.

Sharpe, G. J. & Short M. 2002 Detonation ignition from a temperature gradient for a two-step chain-branching kinetics model. *J. Fluid Mech.* **447**, 31–51.

Sharpe, G. J. & Short M. 2004 Shock-induced ignition of thermally sensitive explosives. *IMA J. Appl. Maths* **69**, 493–520.

Sheffield, S. A., Engelke, R. & Alcon, R. 1989 In-situ study of the chemically driven flow fields in initiating homogeneous and heterogeneous nitromethane explosives. In *9th Intl Symp. on Detonation*, pp. 39–49. Office of Naval Research Arlington.

Short, M. 2001 A nonlinear evolution equation for pulsating Chapman-Jouguet detonations with chain-branching kinetics. *J. Fluid Mech.* **430**, 381–400.

Short, M. & Bdzil, J. B. 2003 Propagation laws for steady curved detonations with chain-branching kinetics *J. Fluid Mech.* **479**, 39–64.

Short, M. & Dold, J. W. 2002 Weak detonations, their paths and transition to strong detonation. *Combust. Theory Model.* **6**, 279–296.

Short, M., Kapila, A. K. & Quirk, J. J. 1999 The chemical-gas dynamic mechanisms of pulsating detonation wave instability. *Phil. Trans. R. Soc. Lond.* A **357**, 3621–3637.

Short, M. & Quirk, J. J. 1997 On the nonlinear stability and detonability limit of a detonation wave for a three-step chain-branching reaction. *J. Fluid Mech.* **339**, 89–119.

Short, M. & Sharpe, G. J. 2002 Pulsating instability of detonations with a two-step chain-branching reaction model: theory and numerics. *Combust. Theory Model.* **7**, 401–416.

Short, M. & Sharpe, G. J. 2005 Failure and ignition limits of three-step chain-branching detonations. *Combust. Theory Model.* (submitted).

Singh, G. & Clarke, J. F. 1992 Transient phenomena in the initiation of a mechanically driven plane detonation. *Proc. R. Soc. Lond.* A **438**, 23–46.

Varatharajan, B. & Williams, F. A. 2001 Chemical-kinetic descriptions of high-temperature ignition and detonation of acetylene-oxygen-diluent mixtures *Combust. Flame* **125**, 624–645.